

**Project PAJex1
Report No 5**

**Temperature
Dependence of the
Properties of an
Epoxy Adhesive**

L Crocker and G Dean

August 2001

**TEMPERATURE DEPENDENCE OF THE
PROPERTIES OF AN EPOXY ADHESIVE**

L Crocker and G Dean

Materials Centre, National Physical Laboratory
Teddington, Middlesex TW11 0LW

SUMMARY

The work reported here is concerned with comparing the behaviour of a toughened epoxy adhesive at two temperatures, 23°C and 0°C. Tensile and shear tests have been carried out on bulk samples at 23°C and 0°C. A wide range of deformation speeds has been employed in these tests to determine the strain rate dependence of the mechanical properties. The results obtained at the two temperatures have been compared. It was found to be more difficult to obtain reliable data at 0°C.

The experimental data have been used to calculate FE parameters for both the linear and exponent forms of the Drucker-Prager materials model. The calculation of these parameters is explained in detail. Problems with the calculation of parameters at 0°C are highlighted, and a possible solution presented.

Predictions of force against extension were made for a lap-joint specimen using 23°C and 0°C FE parameters. Solutions were obtained over a range of loading speeds using static and dynamic analyses with standard and explicit solvers. Predictions are compared with experimental data that had been obtained at 23°C and 0°C over a range of loading rates. Possible explanations for the differences between measured and predicted force/extension curves are outlined.

© Crown copyright 2001
Reproduced by permission of the Controller of HMSO

ISSN 1473-2734

National Physical Laboratory
Teddington, Middlesex, UK, TW11 0LW

Extracts from this report may be reproduced provided that the source is acknowledged
and the extract is not taken out of context.

Approved on behalf of Managing Director, NPL, by Dr C Lea,
Head of NPL Materials Centre

CONTENTS

1.	INTRODUCTION.....	1
2.	MATERIAL.....	1
3.	BULK SPECIMEN TESTING.....	2
3.1	BULK SPECIMENS AT 23°C.....	2
	3.1.1 Tensile Measurements.....	2
	3.1.2 Shear Measurements.....	2
3.2	BULK SPECIMENS AT 0°C.....	3
3.3	COMPARISON OF 23°C AND 0°C DATA.....	3
	3.3.1 Tensile Data.....	3
	3.3.2 Shear Data.....	4
4.	DETERMINATION OF MATERIAL PARAMETERS.....	4
4.1	MATERIALS MODELS.....	4
4.2	DETERMINATION OF PARAMETERS AT 23°C.....	5
	4.2.1 Linear Drucker-Prager.....	5
	4.2.2 Exponent Drucker-Prager.....	8
4.3	CALCULATION OF PARAMETERS AT 0°C.....	8
5.	FINITE ELEMENT PREDICTIONS OF JOINT PERFORMANCE.....	10
5.1	SPECIMEN GEOMETRY.....	10
5.2	FINITE ELEMENT ANALYSIS.....	10
	5.2.1 Explicit versus implicit analysis.....	10
	5.2.2 Rate-dependent analyses of lap-joint specimens tested at 23°C.....	10
	5.2.3 Rate-dependent analyses of lap-joint specimens tested at 0°C.....	11
6.	EXPERIMENTAL TESTS OF JOINT SPECIMENS.....	12
7.	COMPARISON OF MEASURED AND PREDICTED JOINT PERFORMANCE.....	12
7.1	JOINT TESTS AT 23°C.....	12
7.2	JOINT TESTS AT 0°C.....	13
8.	CONCLUSIONS.....	14
	ACKNOWLEDGEMENTS.....	15
	REFERENCES.....	15

1. INTRODUCTION

Toughened adhesives are ductile materials that can deform to large strains before failure. This ductility allows bonded structures to sustain loads and deformations significantly above those required under normal service conditions. Under severe conditions, such as impact, failure of a bond will be induced by initiation and propagation of a crack leading to reduced load-bearing capability or failure.

One of the main aims of the work on toughened adhesives within the Performance of Adhesive Joints (PAJ) programme has been to use finite element (FE) methods to predict the performance and failure of an adhesive joint under different loading speeds. The most recent work has concentrated on the behaviour of a toughened adhesive at a temperature of 23°C.

The objective of the work reported here is to investigate the behaviour of the epoxy adhesive at a lower temperature, and compare this to the behaviour of the adhesive at 23°C both experimentally and with FE predictions. The low temperature chosen for this study was 0°C.

The behaviour of both bulk and joint specimens at these two temperatures is explored. Calculation of the FE parameters is detailed along with the use of these parameters to obtain FE predictions of the behaviour of a lap joint. Comparisons of predicted force/extension curves are made with experimental results obtained with the epoxy adhesive. Some of the work carried out regarding the epoxy adhesive tested at 23°C has been reported previously⁽¹⁾ but is presented here with a more in-depth discussion of the experimental data used to obtain the Drucker-Prager parameters.

2. MATERIAL

The adhesive chosen for this study was a one part, toughened epoxy supplied by Ford Ltd. Bulk specimens were cut from sheets of 3 mm nominal thickness prepared using procedures described in earlier work⁽²⁾. The bulk specimen sheets were cured for 40 minutes in an oven that had been pre-heated to 180°C, and then air-cooled. Lap-joint specimens were prepared with an adhesive thickness of 0.5 mm. The joint specimens were prepared in an alignment frame and, because of the greater mass of metal, were cured at 180°C for 80 minutes before air-cooling.

The properties of the epoxy adhesive required for finite element analyses have been determined from tensile and shear tests on bulk specimens at two temperatures: 23°C and 0°C. For the tensile tests, both standard dumbbell-shaped specimens (ISO 3167)⁽³⁾ and small dumbbell-shaped specimens (ISO 527-2)⁽⁴⁾ were machined from the sheets. The larger tensile samples give the most accurate strain measurements and were used for lower rate tests. The small tensile samples were used for the higher rate tests as they fit the higher rate test machine. For the shear measurements, Arcan V-notched square plates⁽⁵⁾ were also machined from the sheets. The measurement of tensile and shear properties at 23°C and 0°C are described in sections 3.1 and 3.2.

3. BULK SPECIMEN TESTING

3.1 BULK SPECIMENS AT 23°C

3.1.1 Tensile Measurements

Tensile tests were carried out using Instron universal test machines. For determination of Young's modulus, longitudinal strains were measured using contacting extensometers developed at NPL⁽⁵⁾. For determination of Poisson's ratio, measurements of transverse strain were made using an Instron 2640-007 clip-on extensometer mounted across the sample width.

For determining the strain-hardening function and associated yield parameters in the non-linear region, strains were measured using a Messphysik ME64 video extensometer. This device is non-contacting, thereby avoiding the risk of premature failure initiation, which could occur with contacting extensometers. With this extensometer a video camera with zoom lens is used to generate an image of the specimen on a computer screen. The distance between gauge marks on the specimen surface is determined from the number of pixels between the marks. Strains are calculated from the changes in this distance during the test. Simultaneous measurement of axial and transverse strains enable determination of Poisson's ratio at large extensions.

Samples were tested over a range of loading speeds. Large tensile test pieces were tested at 1 mm/min, 10 mm/min and 100 mm/min using an Instron 4500 series machine. Figure 1 shows the typical stress-strain curves obtained from large tensile samples tested at these three rates. Small tensile test pieces were loaded at 0.1 mm/s, 1 mm/s, 10 mm/s, 100 mm/s and 1000 mm/s using an Instron 1343 servohydraulic test machine. Test methods and measurement of force and extension has been reported previously⁽⁶⁾. The stress-strain curves obtained from the small tensile samples are shown in figure 2. The selected loading speeds produce strain rates in the range $2 \times 10^{-4} \text{ s}^{-1}$ to $2 \times 10^{-2} \text{ s}^{-1}$ for the large tensile samples, and $2.5 \times 10^{-3} \text{ s}^{-1}$ to 25 s^{-1} for the small tensile samples. Figures 1 and 2 show clearly that, at 23°C, there is strain-rate dependence in the tensile behaviour of the epoxy adhesive. The data obtained at each loading rate is reasonably repeatable, especially for the large tensile samples (with slower loading rates). The maximum strain to failure observed was just over 0.08.

3.1.2 Shear Measurements

In the shear tests notched-plate shear (Arcan) specimens were loaded in an Instron machine parallel to the vertical axis joining the V-notches (see figure 3). Shear stresses were calculated from the applied load divided by the cross-sectional area between notches (notch separation times specimen thickness). The shear strains were calculated from the relative vertical displacement of two points equally spaced each side of the centre of the specimen. The point separation was 3 mm. The displacement was determined by an extensometer containing two pivoted lever arms each of which contacted the specimen at one of the two points⁽⁷⁾.

Shear tests were performed at cross-head speeds of 0.2, 2 and 20 mm/min. These speeds were chosen to give effective strain rates in the plastic region that were approximately equal to the effective plastic strain rates in the 1, 10 and 100 mm/min tensile tests. Figure 4 shows typical shear stress-shear strain data obtained at these three rates. Similar to the tensile data, the shear

data also exhibit strain-rate sensitivity in the stress-strain curves. The maximum shear strain at failure is just over 0.14, with the majority of samples failing at strains between 0.1 and 0.14.

3.2 BULK SPECIMENS AT 0°C

To investigate temperature effects, tensile and shear measurements were also carried out at a lower temperature, 0°C, using the methods described above. Both small and large tensile samples were tested using loading rate ranges of 0.1mm/s to 1000 mm/s and 1 mm/min to 100 mm/min respectively. Plots of stress-strain data obtained from large tensile samples tested at 0°C are shown in figure 5, while data from the small tensile samples are plotted in figure 6. Unsurprisingly, all the tensile samples failed earlier at 0°C than they had at 23°C, showing a maximum failure strain of 0.07. The majority of samples failed at a strain of less than 0.06, with many failing at around 0.04 strain. Due to this early failure, the data do not tend to exhibit the plateau in stress values observed in samples tested at 23°C. At 0°C the tensile tests still produce repeatable data, similar to that observed at 23°C.

Arcan shear specimens were tested at 0°C using loading rates of 0.2 mm/min, 2 mm/min and 20 mm/min. The shear stress-shear strain data obtained from these 0°C shear tests are shown in figure 7. It appears that samples tested at 0°C produce quite different data to those obtained at 23°C. Figure 7 shows that at 0°C the shear tests appear to produce less reliable data, there is a large spread of data at all three rates, with no obvious rate dependence. Most of the specimens fail at a shear strain in the region of 0.08 – 0.09. A few specimens sustain load until a shear strain of approximately 0.12, which is a similar failure strain to that observed in the 23°C shear samples. Although the specimens had a range of failure strains, the failure stresses for all loading rates were quite consistent, with all but one of the samples failing between 43 MPa and 47 MPa.

3.3 COMPARISON OF 23°C AND 0°C DATA

3.3.1 Tensile Data

The data obtained for all bulk tests under the two different test temperature conditions have been compared to investigate any temperature effects. Figures 8 and 9 show the comparison of 23°C and 0°C data for large tensile and small tensile specimens respectively. In both figures a typical stress-strain curve has been selected for each loading rate. For each tensile specimen size it can be seen that both the 23°C data and 0°C data show similar strain-rate trends i.e. comparable size steps between the different rate curves. There is clear temperature dependence of the tensile stresses obtained in the non-linear regions of the curves. In the linear regions, there is little difference between modulus values at 23° and 0° as expected for a glassy polymer at temperatures well below the glass to rubber transition temperature, 112°C. For the large tensile samples (figure 8) there is an average increase in failure stress of 13 MPa, for each of the three rates, as the temperature is lowered to 0°C. For the small tensile samples (figure 9) there is an average increase in failure stress of 17 MPa. From the large tensile data it would appear that the strain to failure is reduced at lower temperatures. In the small tensile samples this trend is not observed, indeed some of the 0°C samples reach higher strains before failure than the corresponding 23°C samples. The larger the specimen, the greater the chance it will contain a void. The early failure of large specimens at low temperatures may indicate greater sensitivity to voids at lower temperatures. The small

tensile specimens are less likely to contain voids and therefore the materials sensitivity to voids at lower temperatures is less apparent.

3.3.2 Shear Data

Arcan shear data obtained over three loading rates at a testing temperature of 23°C were found to be very reproducible with very little spread in data (figure 4). But data obtained at 0°C showed a high degree of scatter for all three rates (figure 7). In figure 10 the shear data obtained at 23°C are compared to those acquired at 0°C. For this figure, a typical curve representing the shear stress-shear strain behaviour at 23°C has been selected for each loading rate. At 0°C it is difficult to select a ‘typical’ shear stress-shear strain curve so, for the purpose of this comparison, curves whose shear modulus values match the 23°C shear moduli have been selected. After this careful curve selection it appears that a strain-rate dependence is visible but, taking into account the spread of data at 0°C, this is not wholly reasonable. There is, however, a noticeable difference in the shape of the 23°C and 0°C shear stress-shear strain curves. The curves obtained at 23°C show a large non-linear region, while the 0°C curves are more linear up to failure. This can be explained by the fact that the 0°C samples failed early, before they have exhibited much non-linear behaviour. If the samples had reached higher strains before failure, it is expected that the stress-strain curves would be of a similar shape to the 23°C curves and simply reach higher flow stresses much like the 0°C tensile samples.

4 DETERMINATION OF MATERIAL PARAMETERS

4.1 MATERIALS MODELS

At both 23°C and 0°C, the epoxy adhesive studied is a ductile material that exhibits yielding and plastic flow in tension before failing at tensile strains of just under 0.1. Hence, for the purpose of finite element analysis, elastic-plastic models have been used to describe the deformation behaviour. FE analyses have been carried out with ABAQUS⁽⁸⁾ FE software using two forms of the Drucker-Prager materials model: the linear and exponent forms. In both of these models calculations of stress and strain distributions at low strains are based on the theory of linear elasticity. Hence, the linear elastic behaviour of the material is characterised by the Young’s modulus E and the Poisson’s ratio ν_e . The onset of non-linearity in a stress-strain curve is due to plastic deformation and occurs at the first yield stress. The subsequent increase in stress with strain is associated with the effects of strain hardening, and stress calculations involve the use of a yield criterion. The two Drucker-Prager models differ in the form of yield criterion employed⁽⁸⁾.

The most commonly used elastic-plastic model is based on the von Mises yield criterion, but it is known that the von Mises criterion is not an accurate description of yielding in adhesives where plasticity is sensitive to the hydrostatic component of stress as well as the shear component⁽⁹⁾. The simplest yield criterion that includes hydrostatic stress sensitivity is a modification of the von Mises criterion, and is shown below

$$\sigma_T = \frac{\sqrt{3}(\lambda+1)}{2\lambda} J_{2D}^{1/2} + \frac{(\lambda-1)}{2\lambda} J_1 \quad (1)$$

where σ_T is a yield stress in tension and is a material property. λ is a measure of the sensitivity of yielding to the hydrostatic stress (see section 4.2.1). $J_{2D}^{1/2}$ is the second invariant of the deviatoric stress tensor and is a measure of the effective shear stress applied to the material. J_1 is the first invariant of the stress tensor and is equal to 3 times the hydrostatic component of stress.

In ABAQUS, the criterion shown in equation (1) is used in the linear Drucker-Prager model and takes the form

$$d = q - p \tan \beta \quad (2)$$

where

$$d = \frac{2\lambda\sigma_T}{(\lambda+1)}, \quad p = -\frac{J_1}{3}, \quad q = \sqrt{3}J_{2D}^{1/2}$$

and

$$\tan \beta = \frac{3(\lambda-1)}{(\lambda+1)} \quad (3)$$

The flow parameter, ψ , is also required for this model and this is calculated from measurements of the plastic component of Poisson's ratio, ν_p , as follows

$$\tan \psi = \frac{3(1-2\nu_p)}{2(1+\nu_p)} \quad (4)$$

If $\tan \psi = \tan \beta$ then flow is associated.

An alternative yield criterion that is sensitive to hydrostatic stress is

$$\lambda\sigma_T^2 = 3J_{2D} + (\lambda-1)\sigma_T J_1 \quad (5)$$

In ABAQUS, this criterion is used in the exponent Drucker-Prager model and is described by the equation

$$a q^2 = p + p_t \quad (6)$$

where

$$a = \frac{\sigma_T}{3(3\sigma_S^2 - \sigma_T^2)} \quad (7)$$

and

$$p_t = a\sigma_T^2 + \frac{\sigma_T}{3} \quad (8)$$

σ_S and σ_T are yield stresses obtained at the same effective plastic strain.

4.2 DETERMINATION OF PARAMETERS AT 23°C

4.2.1 Linear Drucker-Prager

The parameters required for the linear Drucker-Prager model are E , ν_e , K , β , ψ and the strain hardening function $\sigma_T(\epsilon_p)$. The Young's modulus and Poisson's ratio are obtained from measurements of stress-strain and lateral strain in tensile tests on bulk specimens at small strains where the stress-strain plot is linear e.g. up to a strain of about 0.01 in figure 1. These

elastic properties were observed to depend slightly on strain rate. Data for a single strain rate of $2 \times 10^{-3} \text{ s}^{-1}$ were used to calculate the parameters at 23°C. The parameter K is the ratio of the flow stress in triaxial tension to the flow stress in triaxial compression. The default value for K is assumed to be 1.

The parameter β is calculated from equation (3). This requires knowledge of the parameter λ . λ is equal to the ratio of yield stresses in compression and tension at the same equivalent plastic strain. The determination of λ requires measurements of yield behaviour under two different states of stress. If stress-strain data are available under both compression and tension, λ may be calculated directly. For this work, values of λ have been determined from a combination of tension and shear tests, due to difficulties associated with uniaxial compression tests. λ can be obtained by rearranging equation (1). In a tensile test $J_{2D}^{1/2} = \sigma_T/\sqrt{3}$ and $J_1 = \sigma_T$, while in a shear test $J_{2D}^{1/2} = \sigma_s$ and $J_1 = 0$. Substituting these into equation (1) gives

$$\lambda = \frac{\sqrt{3}(\sigma_s / \sigma_T)}{2 - \sqrt{3}(\sigma_s / \sigma_T)} \quad (9)$$

where σ_s and σ_T are yield stresses obtained at the same effective plastic strain, $\bar{\epsilon}_p$, from stress/strain curves measured in shear and tension at the same effective plastic strain rate, $\dot{\bar{\epsilon}}_p$. The definition of effective plastic strain used here is

$$\bar{\epsilon}_p = \frac{2}{\sqrt{3}} I_{2D}^{1/2} \quad (10)$$

where $I_{2D}^{1/2} = \left\{ \frac{1}{6} [(\epsilon_{p1} - \epsilon_{p2})^2 + (\epsilon_{p2} - \epsilon_{p3})^2 + (\epsilon_{p3} - \epsilon_{p1})^2] \right\}^{1/2}$

and ϵ_{p1} , ϵ_{p2} and ϵ_{p3} are components of principal plastic strain. It follows that under uniaxial tension

$$\bar{\epsilon}_p = \frac{2}{3} (1 + \nu_p) \epsilon_{pT} \quad (11)$$

and in shear

$$\bar{\epsilon}_p = \frac{\gamma_p}{\sqrt{3}} \quad (12)$$

where γ_p is the plastic component of the engineering shear strain and is equal to twice the plastic component of the tensor shear strain. The effective yield stress $\bar{\sigma}$ is given by the expression

$$\bar{\sigma} = \sqrt{3} J_{2D}^{1/2} = q \quad (13)$$

In tension

$$\bar{\sigma} = \sigma_T, \text{ the tensile yield stress} \quad (14)$$

and in shear

$$\bar{\sigma} = \sqrt{3} \sigma_s \quad (15)$$

Figure 11 shows true stress/true strain curves measured in tension and shear on bulk specimens. The test speeds chosen gave the same effective plastic strain rates in both tests. Using equations (11) to (15), the measured stress/strain curves in tension and shear shown in figure 11 have been plotted on axes of effective stress against effective plastic strain, see figure 12. Determination of the value used for ν_p is discussed below. Values for $\sqrt{3}\sigma_s$ and σ_T must be obtained at the same effective plastic strain. In this case, values of $\sqrt{3}\sigma_s = 73 \text{ MPa}$

($\sigma_s = 42$ MPa) and $\sigma_T = 57$ MPa were obtained at an effective plastic strain of 0.03. Hence, λ can be calculated using these values in equation (9) and then β can be obtained using equation (3). The obtained λ value of 1.76 (see table 1) is high. This is due to the presence of cavities that are nucleated in this rubber-toughened epoxy adhesive under a tensile stress.

Determination of ψ requires measurement of longitudinal and lateral true strain throughout the non-linear region of a tensile test. The tensile test was conducted at a speed that will give the same strain rate as that used to obtain the data used for the calculation of β ($2 \times 10^{-3} \text{ s}^{-1}$). The true plastic component, v_p , of Poisson's ratio can be deduced from the ratio of true transverse plastic strain to the true longitudinal plastic strain. There was a variation of v_p with longitudinal plastic strain, so a representative value of 0.29 was selected. This value is used in equation (4) to determine ψ . The table below shows the linear Drucker-Prager parameters calculated using data obtained at 23°C and a strain rate of $2 \times 10^{-1} \text{ s}^{-1}$.

Table 1. Linear Drucker-Prager parameters for the epoxy adhesive at 23°C

E (GPa)	v_e	λ	$\beta(^{\circ})$	K	v_p	$\psi(^{\circ})$
2.97	0.35	1.76	40	1	0.29	26

The strain hardening function, $\sigma_T(\epsilon_p)$, is obtained from measurements of tensile yield stress σ_T and plastic strain ϵ_p in a uniaxial tension test at strains ranging from that associated with the onset of non-linearity up to the failure strain. For strains above the linear range, the stress σ is identified with the yield stress σ_T and the true plastic strain component was calculated from the measured true strain assuming additivity of the elastic and plastic components⁽⁹⁾.

With the parameters in table 1, it is possible to use finite element analysis to calculate the deformation of a joint at a speed that gives an effective strain rate in the adhesive equivalent to those of the test data used to derive the parameters. The behaviour at other speeds can be determined with knowledge of the rate-dependent nature of the bulk adhesive. The main rate-dependent property that can be incorporated into ABAQUS is the strain hardening function. The other parameters show very little rate-dependence. Hence, the hardening function was determined over a range of strain rates, and data for the epoxy at 23°C are shown in figure 13. These hardening curves can be used to predict joint behaviour at speeds up to approximately 10 mm/s. In order to predict joint performance at speeds of up to 1m/s, hardening curves are required at higher strain rates. For this purpose, the hardening curves in figure 13 have been modelled using an empirical function⁽¹⁾. The function used is

$$\sigma_T = [\sigma_0 + (\sigma_f - \sigma_0)(1 - \exp(-(\epsilon_p / \epsilon_{ps})^n))] (1 + \alpha \epsilon_p) \quad (16)$$

With this function, the yield stresses σ_T increase from σ_0 (the first yield stress) corresponding to zero plastic strain to a value of σ_f (the initial flow stress) corresponding approximately to the plateau stress. The parameter ϵ_{ps} represents some mean strain where the stress is rising rapidly between σ_0 and σ_f . The parameter n influences the strain range over which the rise in stress occurs. The term containing the parameter α describes a small increase of σ_T with plastic strain during flow. A curve was fitted to each set of data with a unique set of parameters, producing very good fits. The parameters ϵ_{ps} , n and α were found to be essentially rate independent for this material and so, for the tensile test data, are assumed to

take average values of 0.005, 0.6 and 0.85 respectively without significant loss of predictive accuracy. The values of σ_0 and σ_f were extrapolated using a form of the Eyring equation⁽¹⁾. The predicted hardening curves are compared with the experimental data in figure 13, and are seen to be satisfactory. Also shown in figure 13 are predicted hardening curves for strain rates of 250 s^{-1} and 2500 s^{-1} . These strain rates are beyond the limit for which accurate experimental measurements are possible.

4.2.2 Exponent Drucker-Prager

The parameters required for the exponent Drucker-Prager model are E , ν_e , a , b , ψ and the strain hardening function $\sigma_T(\epsilon_p)$. The determination of Young's modulus, Poisson's ratio, ψ and the strain hardening function has been described in section 4.2.1. The same values of these parameters are used for the exponent Drucker-Prager model. The parameter b determines the shape of the yield surface, and was taken to have a value of 2.

The parameter a is calculated from equation (7) using values for σ_S and σ_T calculated at the same effective plastic strain. For the exponent Drucker-Prager, the values used for σ_S and σ_T are the same as those obtained during calculation of β in the linear Drucker-Prager model i.e. 42 MPa and 57 MPa respectively. The calculated exponent Drucker-Prager parameters are shown in table 2. These parameters were calculated from data obtained at a strain rate of $2 \times 10^{-3} \text{ s}^{-1}$.

Table 2. Exponent Drucker-Prager parameters for the epoxy adhesive at 23°C

E (GPa)	ν_e	a	b	ν_p	$\psi(^{\circ})$
2.97	0.35	0.009	2	0.29	26

4.3 CALCULATION OF PARAMETERS AT 0°C

The parameters for both the linear and exponent forms of the Drucker-Prager model were calculated from data obtained at 0°C using the methods described in sections 4.2.1 and 4.2.2. Data for a single strain rate of $1 \times 10^{-4} \text{ s}^{-1}$ were used to calculate the parameters.

Overall, the calculation of parameters at 23°C was quite straightforward. The bulk data used to obtain the parameters were reliable and reproducible. Both the shear and tensile data flatten out at higher strains. This means that the parameters calculated for the Drucker-Prager model will be roughly constant above plastic strains of approximately 0.025 (see figure 12). But, the calculation of parameters at 0°C was found to be more complex due to the nature of the bulk data. The 0°C tensile specimens failed at relatively low strains and hence small plastic strains. The 0°C shear data were very variable, making it difficult to find a 'typical' curve.

Data obtained at the lowest loading speed were used to calculate the model parameters as the shear tests at this speed produced the smallest spread of data of the three rates tested. Figure 14 shows the measured stress/strain data for tension and shear plotted on axes of effective stress against effective plastic strain. The tensile specimen failed at an effective plastic strain of 0.019. The values for $\sqrt{3}\sigma_S$ and σ_T were obtained at this effective plastic strain producing values of $\sigma_S = 41.8 \text{ MPa}$ and $\sigma_T = 66.5 \text{ MPa}$. Table 3 shows both the linear (E , ν_e , β , ψ) and

exponent (E , ν_e , a , ψ) Drucker-Prager parameters calculated using these data, b was assumed to be 2.

Table 3. Linear and exponent Drucker-Prager parameters for the epoxy adhesive at 0°C

E (GPa)	ν_e	λ	$\beta(^{\circ})$	ν_p	$\psi(^{\circ})$	a
3.08	0.35	1.19	14.9	0.29	26	0.027

Calculations made using these 0°C experimental data were found to produce a low λ value (see table 3) compared to that obtained at 23°C (where $\lambda = 1.76$). A new model being developed⁽¹⁰⁾ that takes into consideration the influence of rubber particle cavitation on plastic deformation predicts that, at plastic strains in tension for which all the rubber particles have cavitated, the ratio $\sqrt{3}\sigma_S/\sigma_T$ will be the same at 23°C and 0°C. From equation (9), the value of λ should also be the same at these temperatures. Therefore, the fact that λ has a low value either implies that not all the rubber particles are cavitating (as $\lambda = 1.19$ is closer to that obtained for material without cavities), or that the experimental data is unreliable. The tensile experimental data appeared reasonable, but the shear data was known to be inconsistent with the 23°C shear data, producing lower shear stresses than expected. The value of σ_S achieved is much lower than the plateau value of σ_S , hence lowering the λ value.

If the value of λ is assumed to be independent of temperature (implying unreliable shear data) it is possible to obtain an alternative set of Drucker-Prager parameters. The following sets of data are considered reliable: - tension at 23°C; shear at 23°C; tension at 0°C. By taking values from these three sets of data at a particular effective plastic strain and assuming the ratio of $\sqrt{3}\sigma_S/\sigma_T$ is the same at 23°C and 0°C, the corresponding shear stress at 0°C can be obtained. This derived value of σ_S at 0°C can then be used, along with σ_T to calculate value of the parameter a at 0°C. This alternative set of Drucker-Prager parameters are given below in table 4.

Table 4. Alternative linear and exponent Drucker-Prager parameters for the epoxy adhesive at 0°C, calculated using a derived shear curve.

E (GPa)	ν_e	λ	$\beta(^{\circ})$	ν_p	$\psi(^{\circ})$	a
3.08	0.35	1.76	40	0.29	26	0.0076

The linear Drucker-Prager parameters at 0°C are now the same as those obtained at 23°C (table 1), the only difference being the hardening curves. The exponent Drucker-Prager parameter a is lower at 0°C than at 23°C.

Strain hardening curves for the epoxy at 0°C were obtained over a range of strain rates. These curves are shown in figure 15. As before, the experimental curves were fitted with the empirical function described in equation (16) and a form of the Eyring equation was used to describe the rate dependence of σ_0 and $\sigma_f^{(1)}$. These fits are also shown in figure 15. Average values for the parameters ϵ_{ps} , n and α were selected and these were used to predict higher rate curves. Figure 16 shows the fits to the experimental data using the average parameters and also the higher rate (250 & 2500 s⁻¹) predicted curves.

5. FINITE ELEMENT PREDICTIONS OF JOINT PERFORMANCE

5.1 SPECIMEN GEOMETRY

A lap shear test specimen was chosen for the comparison of measured and predicted joint behaviour. A diagram showing the geometry and dimensions of the specimen is shown in figure 17. Geometric singularities have been removed by incorporating a radius on the edges at the end of each adherend, and a circular fillet on each end of the adhesive. The lapjoint was meshed using the pre-processor FEMGV. The ABAQUS continuum 2-D solid plane strain elements (CPE4R)⁽⁵⁾ were used. Predictions were obtained using the mesh shown in figure 18. Mesh density can affect the strain predictions in regions of strain concentration⁽¹⁾: a smaller element size will generally give a higher maximum strain although at very small element sizes, further dimension changes cause little effect. In this work it is the force-extension curves that are of interest. Force-extension curves are independent of mesh density hence the mesh used was relatively coarse, reducing the analysis run time considerably. In all analyses the steel adherends were assumed to be linear elastic. The boundary conditions were set up such that the nodes along the end of one adherend were completely constrained, while a displacement was applied to the end nodes of the other adherend (displacement control).

5.2 FINITE ELEMENT ANALYSIS

5.2.1 Explicit versus implicit analysis

A dynamic analysis takes into account the rate-dependent behaviour of adhesive properties. In ABAQUS, dynamic analyses can be carried out using either the standard (implicit) solver or the explicit solver. Both methods have advantages and disadvantages. The advantage of using the standard solver is that the initial time increment size can be chosen manually. ABAQUS then uses an automatic time incrementation scheme to adjust the increment size as necessary to obtain solutions. This means that the computer processing times are generally significantly shorter than when using the explicit solver, especially at the lower loading rates. With the explicit solver, the time step is determined by the time for a stress wave to cross the smallest element dimension. The result is that processing times can be excessive, especially when a refined mesh is being used, or when the loading rate is low. The processing time can be reduced by mass scaling i.e. using artificially high values of material density, but care must be taken to ensure that inertial forces still remain insignificant. The main advantage of the explicit code is that solutions can be obtained at larger extensions than can generally be achieved with the standard dynamic analysis. The explicit solver is particularly useful for analysing bonded joints made with tough adhesives that sustain large extensions before failure, such as the epoxy studied here.

5.2.2 Rate-dependent analyses of lap-joint specimens tested at 23°C

Rate-dependent plasticity is implemented in ABAQUS by inputting data for the strain hardening function over a range of strain rates. These data are obtained from tensile tests carried out over a wide range of strain rates as discussed in section 4.2.1. The maximum strain rate obtained experimentally at 23°C was 41 s⁻¹ which corresponds with the mean strain rate in a lapjoint specimen at a loading speed of 10 mm/s. In order to predict joint performance at speeds of up to 1 m/s, it is necessary to extend the strain rate range for these data by a factor of approximately 100. The determination of hardening curves to enable

predictions at these higher speeds has been described in sections 4.2.1 and results are shown in figure 13.

Previous analysis of the results of tensile and shear tests on bulk specimens and tensile butt joint tests have indicated that the deformation behaviour of the epoxy adhesive is best described by the exponent Drucker-Prager model⁽⁹⁾. So an analysis using rate-dependent plasticity was initially run using this model in ABAQUS/Standard. This analysis had convergence problems very early on, and failed to converge at an extension of less than 0.05 mm. These problems indicated that an explicit analysis would be needed to achieve predictions using rate-dependent plasticity at a reasonable extension. As, at the start of the work, the exponent Drucker-Prager model was not available in ABAQUS/Explicit, the linear Drucker-Prager model was used to obtain force/extension curves using rate-dependent plasticity. The predicted force/extension curves for lapjoint loading speeds of 1 mm/s, 10 mm/s and 100 mm/s tested at 23°C were obtained using the linear Drucker-Prager parameters given in table 1. These predictions are shown in figure 19. The extension is obtained from the separation between two nodes on the adherends with an initial gauge length of 25 mm. These two nodes mark the contact positions of the extensometer used during the experimental testing of lap joints (see section 6). Four hardening curves were used, one with a strain rate approximately the same as the average strain rate in the lapjoint, one higher strain rate curve, one lower strain rate curve, and an extremely low strain rate curve which is designated the zero rate curve.

As mentioned above, the most accurate predictions that can be obtained using available models are considered to be those derived using the exponent Drucker-Prager model. Since convergence problems arise when using this model with rate-dependent hardening curves and ABAQUS/standard, predictions have been obtained using a single 'effective' strain hardening curve which gives a comparable force/extension curve to that which would be obtained from an analysis using four hardening curves. New hardening curves were generated at various strain rates using the empirical formula given in equation (16). It was found⁽⁹⁾ that at a lap joint loading speed of 1 mm/s, the explicit rate-dependent predictions compared well with a single rate prediction using a strain rate of 3 s^{-1} (see figure 20).

It is assumed that a factor of 10 increase in loading rate will give a factor of 10 increase in the mean strain rate in the adhesive region of the lapjoint. This assumption is supported by previous work⁽⁹⁾ which has compared force/extension predictions from an explicit analysis with four hardening curves and a loading rate of 0.1 mm/s with the single hardening curve prediction from a standard analysis at a strain rate of 0.3 s^{-1} . It is now possible to run implicit (standard) exponent Drucker-Prager analyses using these mean strain rates to obtain a suite of force/extension predictions over a range of lapjoint loading speeds. These are shown in figure 21. The predicted curves are all evenly spaced, although it is noted that the predictions at lower load rates had convergence problems at lower extensions. The force/extension curve predicted using the Exponent Drucker-Prager model at a loading speed of 1 mm/s is also shown in figure 20 to highlight the difference between linear Drucker-Prager and exponent Drucker-Prager predictions.

5.2.3 Rate-dependent analyses of lap-joint specimens tested at 0°C

Linear Drucker-Prager predictions of force/extension were obtained for a 0°C lap joint test with a loading speed of 1 mm/s using rate-dependent hardening curves in explicit. Two analyses were run using the two sets of parameters given in tables 3 and 4. The two

force/extension curves obtained are shown in figure 22. The analysis run using $\beta = 40^\circ$ ($\lambda = 1.76$) predicted higher loads than those obtained using $\beta = 14.9^\circ$ ($\lambda = 1.19$). These explicit, rate-dependent predictions were matched with those obtained using single rate hardening curves. It was found that, for both sets of parameters, a single rate of 2 s^{-1} gave predictions that correlated with the rate-dependent analyses. These single rate force/extension curves are also shown in figure 22. Once again, it is assumed that a factor of 10 increase in loading rate will give a factor of 10 increase in the mean strain rate in the adhesive region of the lapjoint.

Implicit exponent Drucker-Prager analyses were run using a series of effective hardening curves spanning a range of strain rates to obtain force/extension predictions over a range of loading speeds. The predicted curves obtained using both sets of parameters are shown in figure 23. At 0°C all predictions reach the same extension. This is in contrast to the situation at 23°C where convergence problems were observed at lower loading speeds. The predicted curves using both sets of parameters are all equally spaced, due to the fact that the same series of hardening curves were used in both sets of analyses.

6. EXPERIMENTAL TESTS ON JOINT SPECIMENS

Tensile tests on lap-joint specimens at 23°C and 0°C have been carried out under controlled displacement rate conditions in a servohydraulic test machine. Loading speeds within the range 0.1 mm/s to 100 mm/s were used. The extension of the joint was measured using extensometers (with gauge length of 25 mm) attached to the wide faces of the lap-joint adherends. Two extensometers were used to improve measurement accuracy. A series of force vs extension curves were obtained at different loading speeds. The curves presented in figure 24 (a) and (b) are typical of results obtained from several sets of test specimens at different loading speeds at 23°C and 0°C .

At 23°C (figure 24a) the extension at failure varies between 0.25 mm and 0.45 mm implying a mean shear strain in the adhesive at failure of between 50 and 90%. At 0°C (figure 24b) the failure extension ranges between 0.2 mm and 0.35 mm giving a mean shear strain in the adhesive at failure of between 40 and 70%. Determination of extension at maximum load produces more consistent data. At 23°C , the average extensions at maximum loads are 0.157, 0.181, 0.192 and 0.195 mm for loading rates of 0.1, 1, 10 and 100 mm/s respectively. At 0°C , the average extensions at maximum loads for the same set of loading rates are 0.179, 0.198, 0.189 and 0.159 mm respectively. The shape and spacing of the different rate curves look similar for both temperatures, although at 0°C there is more 'noise' in the force/extension curves at the higher rates. This implies that it is more difficult to get smooth, accurate joint data for high rate tests at low temperatures. The maximum loads observed at 0°C are higher than those obtained for the corresponding loading speeds at 23°C . At both temperatures the force drops gradually, after reaching maximum load, before the lap joint fails.

7. COMPARISON OF MEASURED AND PREDICTED JOINT PERFORMANCE

7.1 JOINT TESTS AT 23°C

The FE analyses produce predictions of lap joint behaviour in the case where the adhesive is a continuum. No cracks, defects or cavities are modelled in the analyses. The discrepancies between predictions and measured data highlight differences between the assumed

(modelled) and actual adhesive joint condition. Studying these differences can increase understanding of lap joint failure modes.

Predicted and measured force/extension curves obtained at 23°C and at deformation speeds of between 0.1 mm/s and 100 mm/s are compared in figure 25. At small extension where the deformation behaviour of the adhesive is linear, the predicted force/extension curves match reasonably well. However at larger extensions the correlation deteriorates. The measured curves become non-linear well before the predicted curves exhibit any non-linear behaviour. The predicted maximum loads are consistently higher than measured loads, with an average difference between peak experimental and predicted loads of 1.39 kN. Also, once the maximum load has been reached, the forces stay at this level until the analysis ends. In other words, the decrease in load observed on the experimental lap joint test is not predicted with FE analysis.

One explanation is that the adhesive is failing locally at the extension where the measured and predicted curves depart. Although, in previous work⁽¹¹⁾, analyses revealed that the maximum strain in the adhesive at the extension at which the measured and predicted force/extension curves started to depart was significantly below the strain level at which rupture could be expected from the results of tensile tests on bulk and butt-joint specimens⁽¹²⁾. It was initially thought that these differences could be due to differences between the adhesive in the lap joint and the tensile samples used to obtain the hardening data⁽¹¹⁾. Subsequent work⁽¹⁾ investigated this possibility but concluded that, within the scope of this work, the tensile properties were insensitive to cure conditions and specimen thickness.

If the adhesive is failing locally, the sequence of events is likely to be early initiation of cracks within the adhesive followed by slow growth of these cracks while the joint is still able to sustain increasing loads. The peak load roughly corresponds to cracking through the fillet. Once the maximum load is reached, the subsequent time to failure is small, as cracks begin to propagate through the thickness and failure is catastrophic. This explanation has been investigated recently⁽¹³⁾, where analyses have simulated the presence of a crack and the effect of its subsequent growth on force/extension predictions. This was done by progressively disconnecting nodes along the probable crack path. The effect of the crack was seen to progressively reduce the load-bearing capability of the joint and bring predictions closer to the experimental result. This is reiterated in figure 26 which shows the effect of different length cracks on the predicted force/extension curve. The experimental prediction is also shown. Photographic evidence of the presence and growth of a crack at 23°C has also been obtained⁽¹³⁾ which supports this explanation.

7.2 JOINT TESTS AT 0°C

In figure 27 measured force/extension curves obtained at 0°C at deformation speeds of between 0.1 mm/s and 100 mm/s are compared with predictions obtained using the exponent Drucker-Prager model and the parameters acquired using the derived shear data ($a = 0.0076$, $\lambda = 1.76$). At low strains there is good correlation between the experimental data and predictions of force/extension behaviour. The divergence between experimental and predicted behaviour is very similar to that observed at 23°C (figure 25). This was expected because the 0°C parameters used for this exponent Drucker-Prager analysis were obtained with a λ value of 1.76, the same as that used for predictions at 23°C. The experimental data deviate from the predictions as the experimental curves exhibit non-linearity before the predicted curves. This deviation from the predictions occurs later i.e. at larger displacements (approximately 0.075

mm) than observed at 23°C where the divergence occurred at approximately 0.05 mm. Once again the predictions gave consistently higher loads than those observed experimentally, with an average difference of 1.69 kN. This is even higher than that seen at 23°C where the average difference was 1.39 kN.

Force/extension predictions obtained using the exponent Drucker-Prager model and the parameters acquired using the experimental shear data ($a = 0.027$, $\lambda = 1.19$) are compared with measured data in figure 28. These predicted curves give better fits, lying much closer to the measured data than the curves obtained using the alternative parameters. The maximum predicted loads are only slightly higher than the peak experimental loads, with an average difference between experimental and predicted loads of only 0.2 kN. The predictions follow the onset of non-linearity in the experimental lap-joint data reasonably well. The experimental curves only begin an obvious deviation from the predictions once the maximum load has been reached. At this point the experimental loads begin to fall before final failure occurs. From this point, the test time to failure is very small i.e. catastrophic failure occurs. This phenomenon is thought to be due to the fast growth of a crack within the adhesive. The FE analyses take no account of crack growth and hence the loads stay constant once the peak load has been achieved. The fact that the predictions mirror the experimental curves up to this point implies that there is very little crack growth at 0°C prior to catastrophic failure. One explanation would be that the initiation of cracks is delayed at lower temperatures, but once a crack has initiated, propagation is fast.

In reality the situation may be somewhere between the two explanations given above. It can be seen from figure 14 that, if the tension data were extrapolated out to higher extensions, the ratio of σ_s/σ_T , and hence λ , would increase. This would put the predicted curves somewhere between the predictions obtained with the two different sets of parameters. This would then imply that some crack initiation occurs at low extensions (although probably at slightly larger extensions than at 23°C), with slow crack propagation before catastrophic failure.

8. CONCLUSIONS

Experimental data on the behaviour of a toughened epoxy adhesive were obtained through testing of both bulk (tension and shear) and lap-joint specimens at two temperatures (23°C and 0°C). It was found to be more difficult to obtain reliable, reproducible shear data at 0°C than at 23°C for this adhesive.

Two forms of the Drucker-Prager model (linear and exponent) have been used with finite element analysis to predict the deformation behaviour of epoxy lap-joint specimens tested at 23°C and 0°C. The experimental data obtained were used to calculate the required FE parameters. Rate-dependent plasticity was modelled by generating tensile data over a range of testing speeds at both 23°C and 0°C.

Two sets of FE parameters were calculated from 0°C data due to uncertainty in the accuracy of the 0°C shear data. Real experimental data produced a set of FE parameters where the value of λ ($\lambda=1.19$) was much lower than that obtained at 23°C ($\lambda=1.76$). The second set of FE parameters were calculated assuming a constant λ ($\lambda=1.76$ i.e. independent of temperature). The consequence of this assumption is that the effective shear stress used to calculate this set of FE parameters was much higher than that observed experimentally (and is therefore non-conservative).

At 23°C, predicted force/extension curves for the lap-joint specimen reach consistently higher maximum loads than those measured experimentally over a range of loading speeds. It is believed that this is due to premature and localised failure of the adhesive at the interface with the adherend.

At 0°C one set of lap-joint predictions was based on parameters calculated partly from derived 0°C shear data, as there was not total confidence in the experimentally obtained shear data. As expected the predictions were similar to those observed at 23°C due to the assumptions made in deriving the 0°C shear curve. A suggested explanation for the difference between prediction and experiment was the early initiation and slow growth of cracks until a peak load is reached. At this point crack propagation accelerates and failure is catastrophic.

The 0°C lap-joint predictions acquired using parameters calculated from the actual 0°C shear data gave a better fit to measured data. An explanation for this was that there was little crack growth before catastrophic failure. If the experimentally obtained shear data are representative of the material behaviour at 0°C, then it would seem that the method of failure in a lap joint changes subtly with temperature, with a delay in crack initiation observed at lower temperatures. It also implies incomplete cavitation of all the rubber particles at the lower temperature.

ACKNOWLEDGEMENTS

The authors wish to acknowledge the contribution to this work from Mr Alan Pearce and Ms Elena Arranz with the testing of the bulk and joint specimens. The work was funded by the Department of Trade and Industry as part of the Performance of Adhesive Joints programme.

REFERENCES

1. Dean, G.D. and Crocker, L.E. Comparison of the Measured and Predicted Deformation of an Adhesively Bonded Lap-Joint Specimen. NPL report CMMT(A)293, 2001.
2. Dean, G.D. and Duncan, B.C. Preparation and Testing of Bulk Specimens of Adhesives. NPL Measurement Good Practice Guide No 17, July 1998.
3. ISO 3167:1993, Plastics – Multipurpose test specimens.
4. ISO 527-2:1993, Plastics – Determination of tensile properties – Part 2: Test conditions for moulding and extrusion plastics.
5. Duncan, B.C. and Tomlins, P.E. Measurement of Strain in Bulk Adhesive Testpieces. NPL report DMM(B)398, 1994.
6. Duncan, B.C. and Pearce A. Comparison of Impact and High Rate Tests for Determining Properties of Adhesives and Polymers Needed for Design Under Impact Loading. NPL report CMMT(A)134, 1999.

7. Duncan, B.C. and Dean, G.D. Test Methods for Determining Shear Property Data for Adhesives Suitable for Design. NPL report CMMT(B)56, 1996.
8. ABAQUS/Standard User and Theory Manuals, version 5.8, HKS Inc, USA, 1998.
9. Dean, G.D., Read, B.E. and Duncan, B.C. An Evaluation of Yield Criteria for Adhesives for Finite Element Analysis. NPL report CMMT(A)117, 1999.
10. Read, B.E., Dean, G.D. and Ferris, D.H. An Elastic-Plastic Model for the Non-Linear Mechanical Behaviour of Rubber-Toughened Adhesives. NPL report CMMT(A)289, 2000
11. Dean, G.D., Lord, G.J. and Duncan, B.C. Comparison of the Measured and Predicted Performance of Adhesive Joints Under Impact. NPL report CMMT(A)198, 1999.
12. Dean, G.D. and Crocker, L.E. A Proposed Failure Criterion for Tough Adhesives. NPL report CMMT(A)158, 1999.
13. Dean, G.D. and Crocker, L.E. Analysis of Joint Tests on an Epoxy Adhesive. NPL report MATC(A)40, 2001.

FIGURES

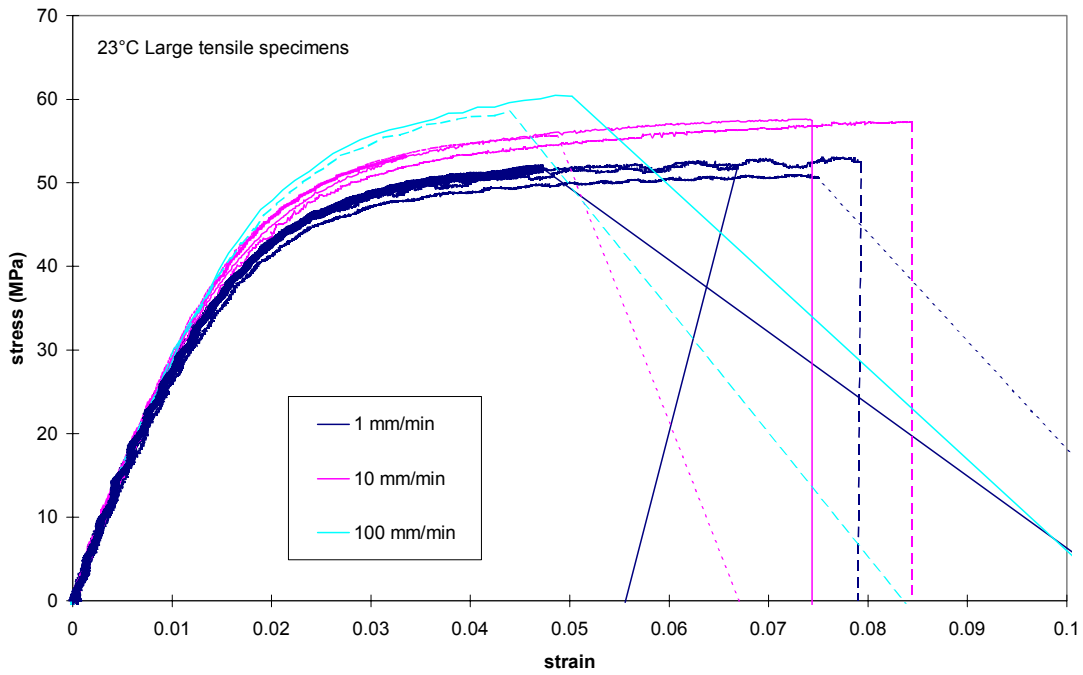


Figure 1. Tensile stress/strain curves for large epoxy tensile specimens tested at 23°C over a range of loading rates.

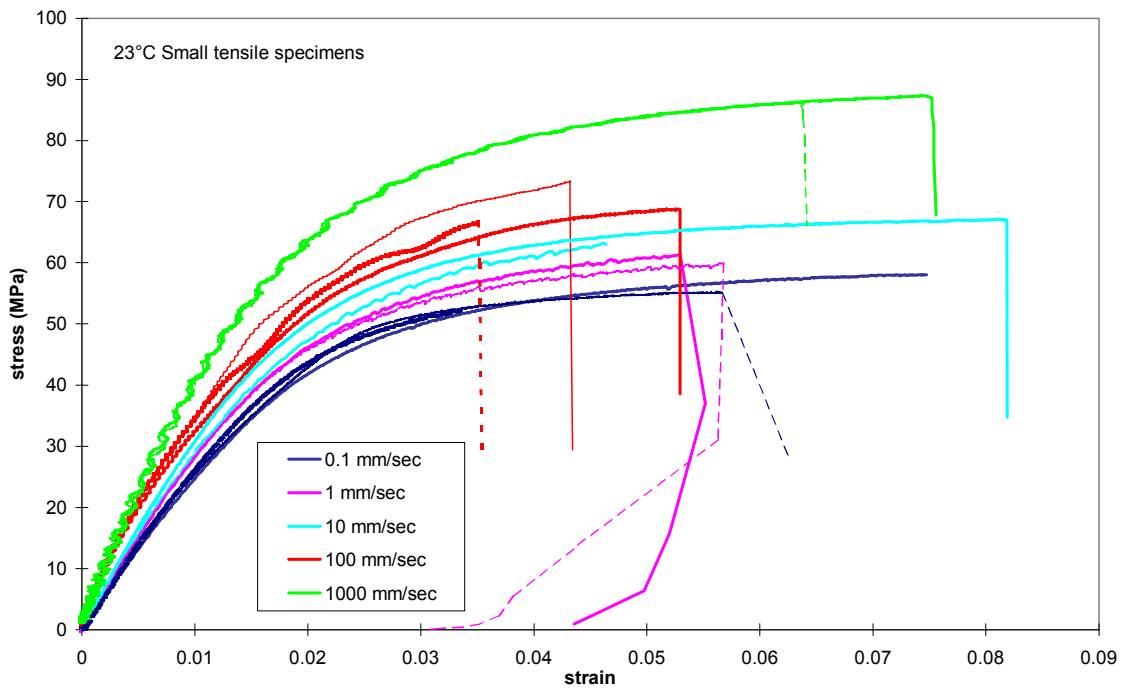


Figure 2. Tensile stress/strain curves for small epoxy tensile specimens tested at 23°C over a range of loading rates.

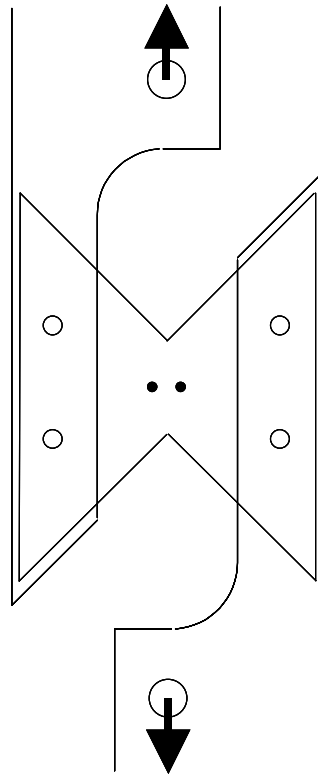


Figure 3. Schematic diagram of an Arcan shear specimen and grips showing the locations of contact points for the extensometer lever arms near the centre of the specimen.

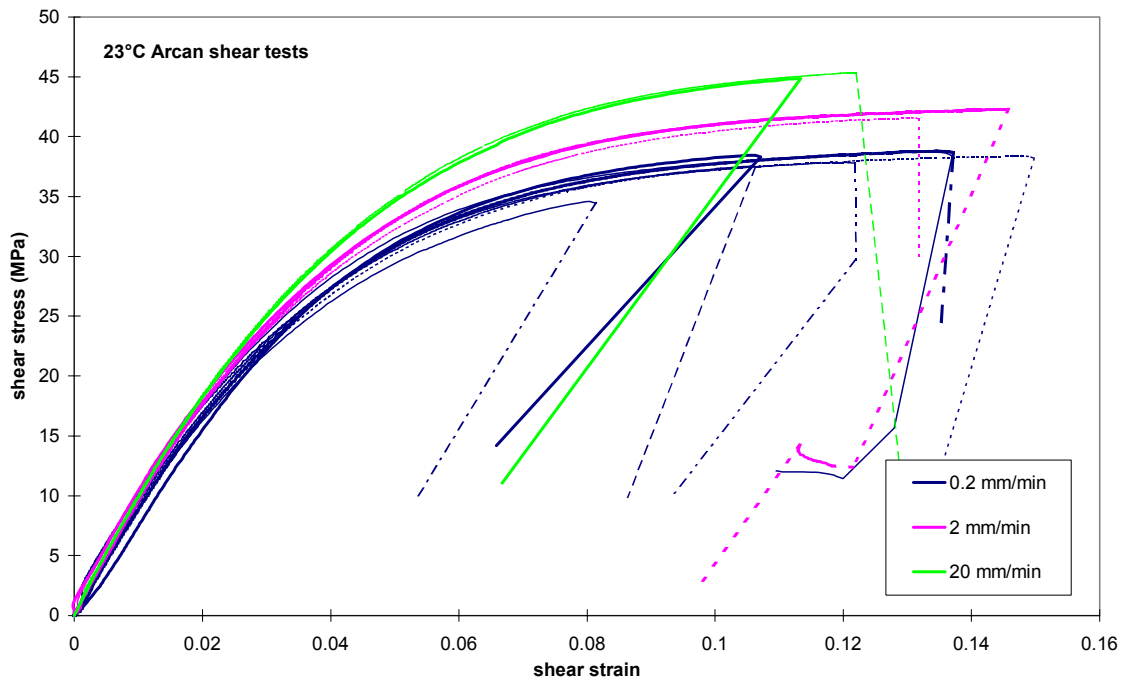


Figure 4. Shear stress/shear strain curves for epoxy Arcan shear specimens tested at 23°C over a range of loading speeds.

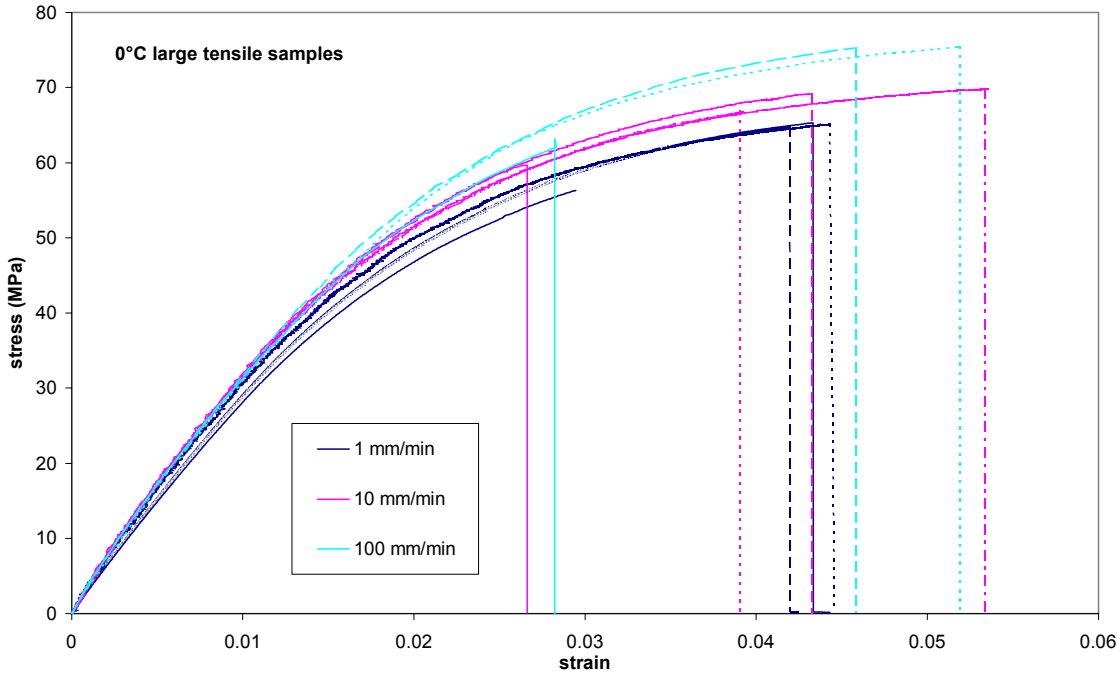


Figure 5. Tensile stress/strain curves for large epoxy tensile specimens measured at 0°C over a range of loading speeds.

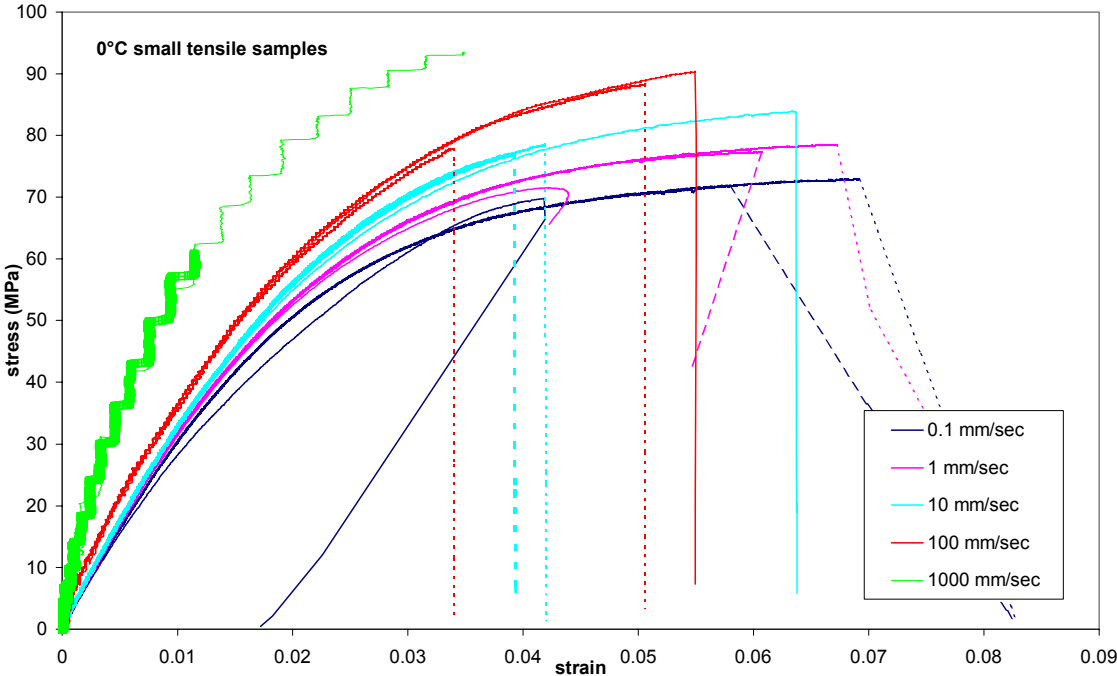


Figure 6. Tensile stress/strain curves for small epoxy tensile specimens measured at 0°C over a range of loading speeds

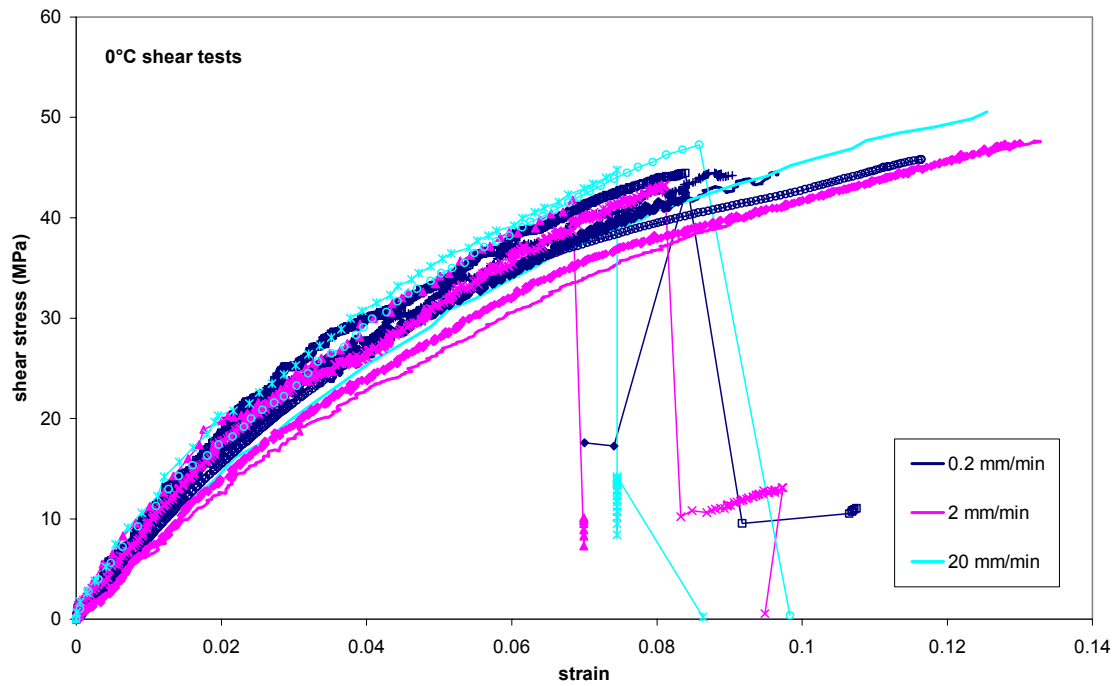


Figure 7. Shear stress/shear strain curves for epoxy Arcan shear specimens tested at 0°C over a range of loading speeds.

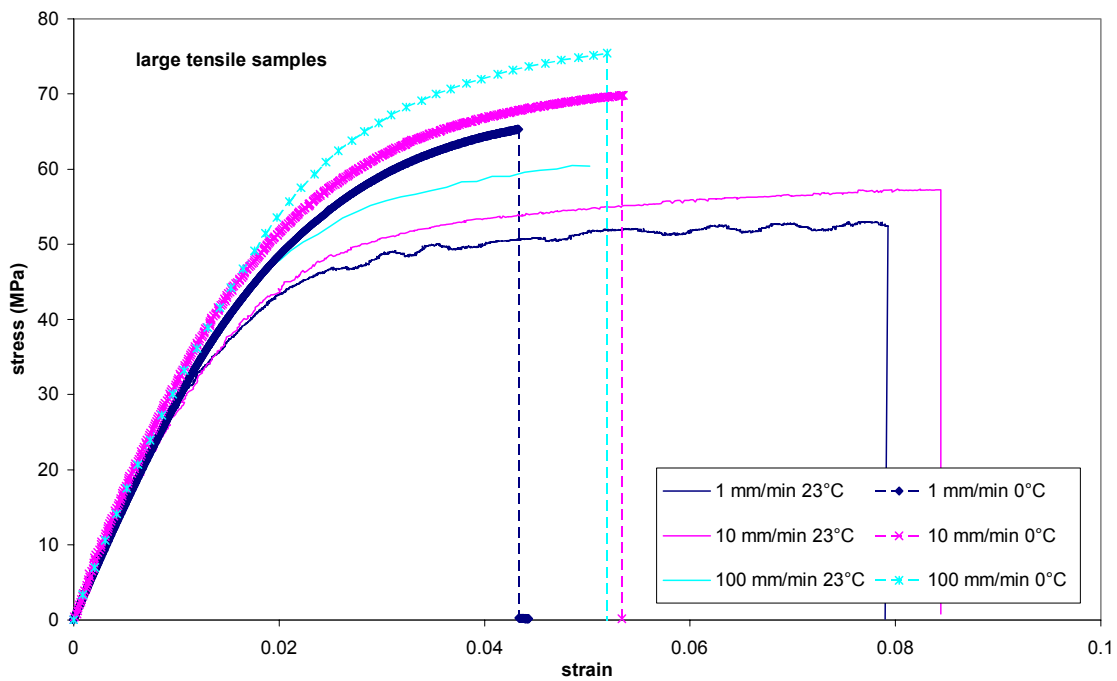


Figure 8. Comparison of 23°C and 0°C tensile data obtained from large epoxy tensile samples over a range of loading speeds.

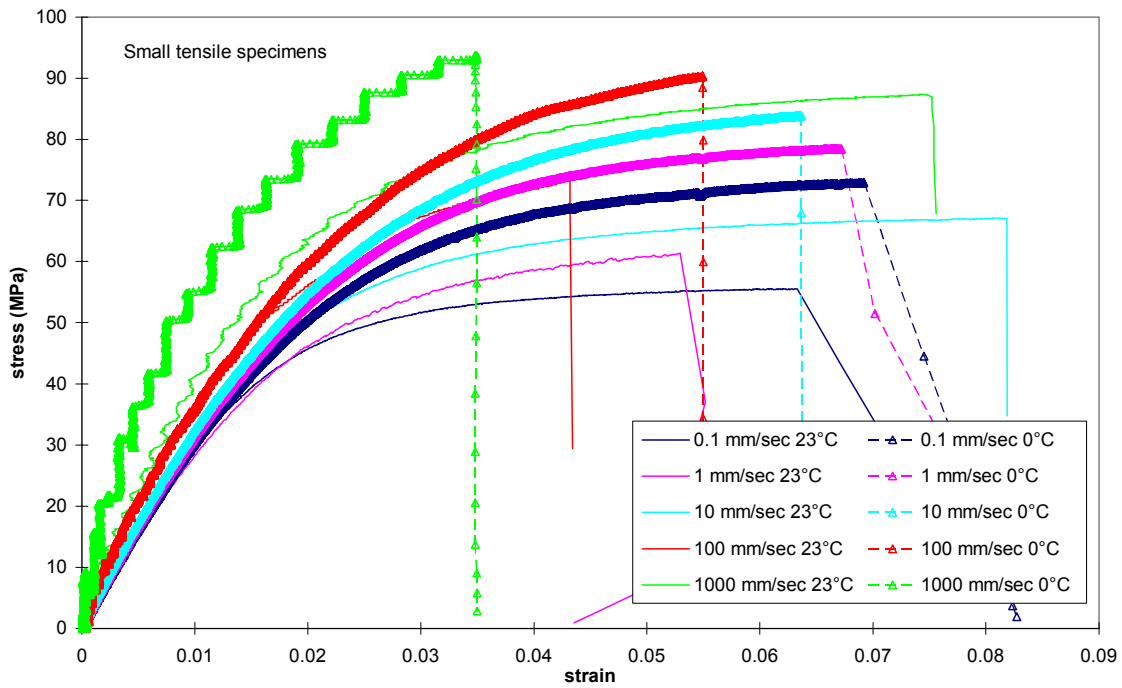


Figure 9. Comparison of 23°C and 0°C tensile data obtained from small epoxy tensile specimens over a range of loading speeds.

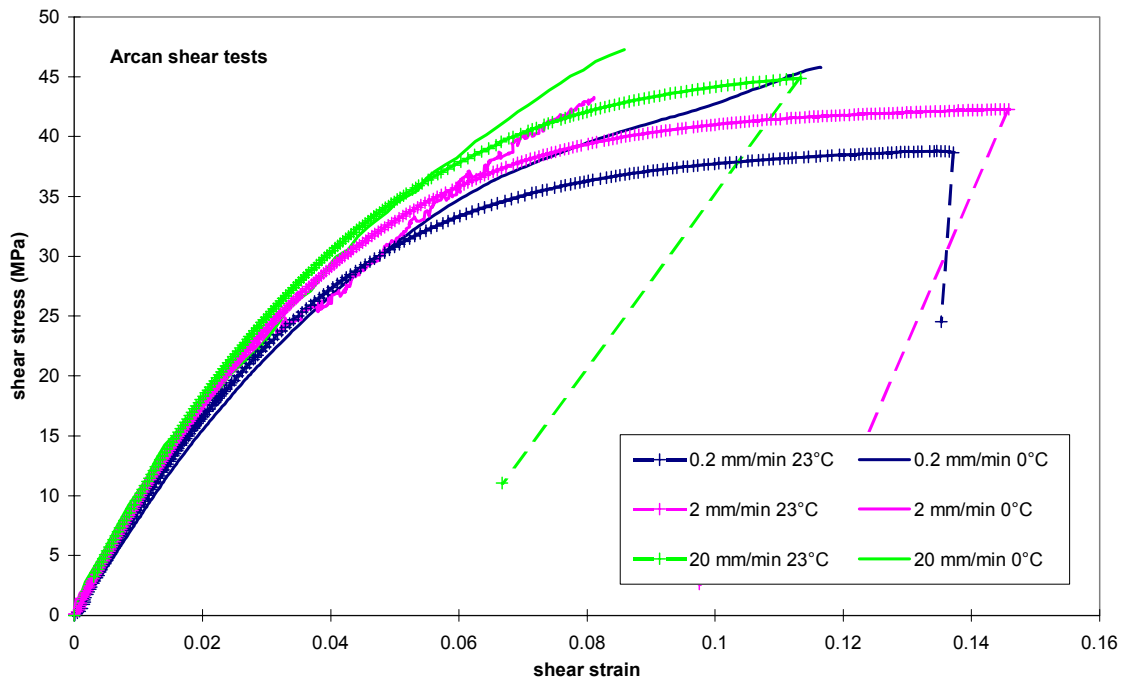


Figure 10. Comparison of 23°C and 0°C shear data obtained from epoxy Arcan shear samples over a range of loading speeds.

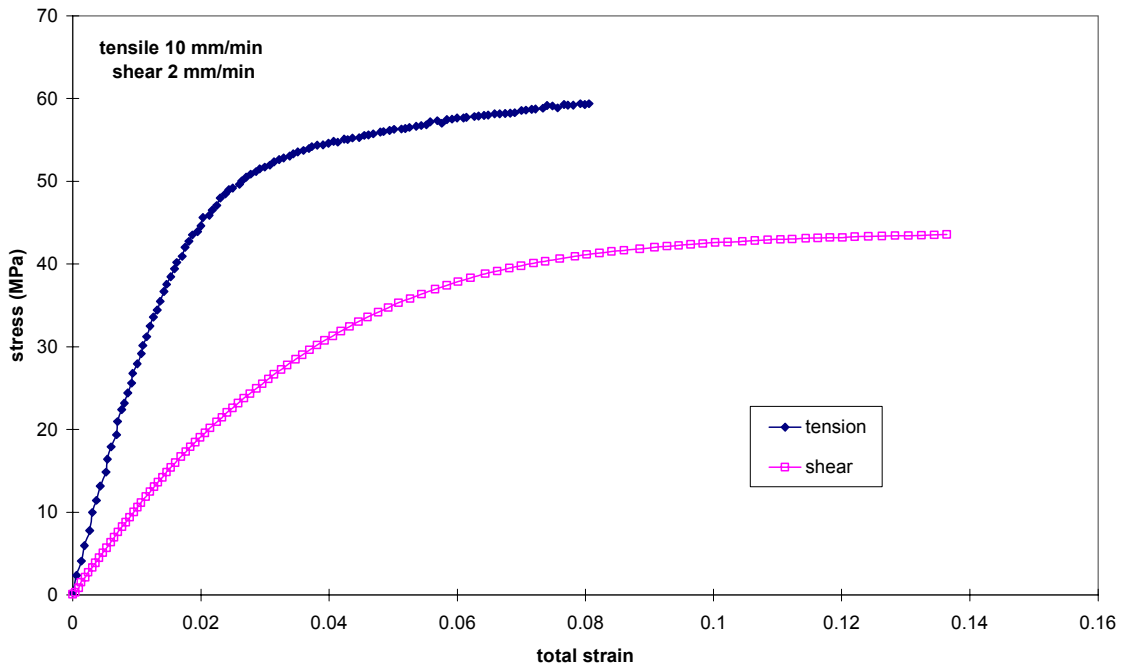


Figure 11. Stress/strain curves for the epoxy adhesive in tension and shear measured at the same effective plastic strain rate of 2.10^{-3} s^{-1} at 23°C .

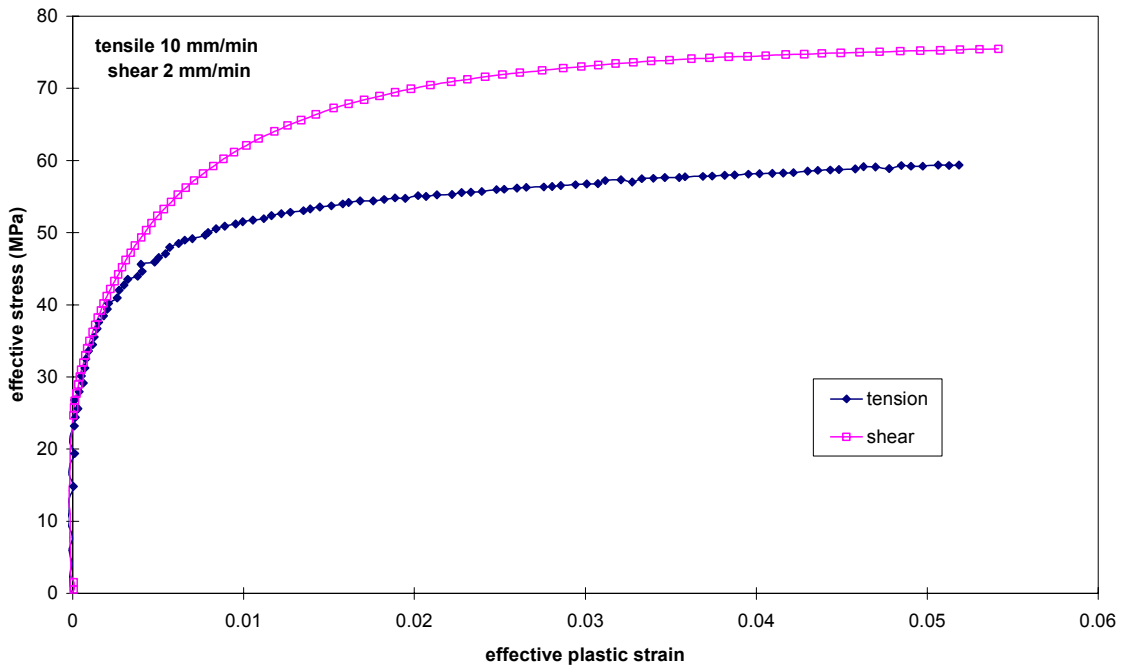


Figure 12. Plots of effective stress against effective plastic strain derived from data in figure 11.

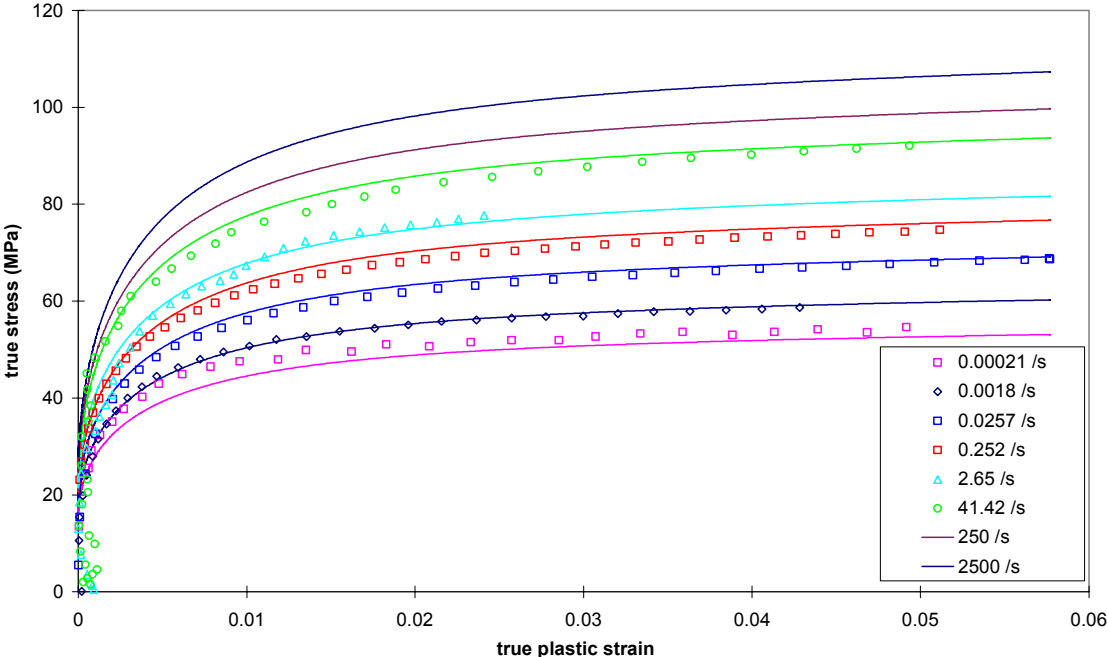


Figure 13. Comparison of 23°C experimental hardening curves (symbols) and fitted hardening curves (solid lines) derived using equation 16 and averaged parameters. Also shown are extrapolated data for strain rates of 250 s⁻¹ and 2500 s⁻¹.

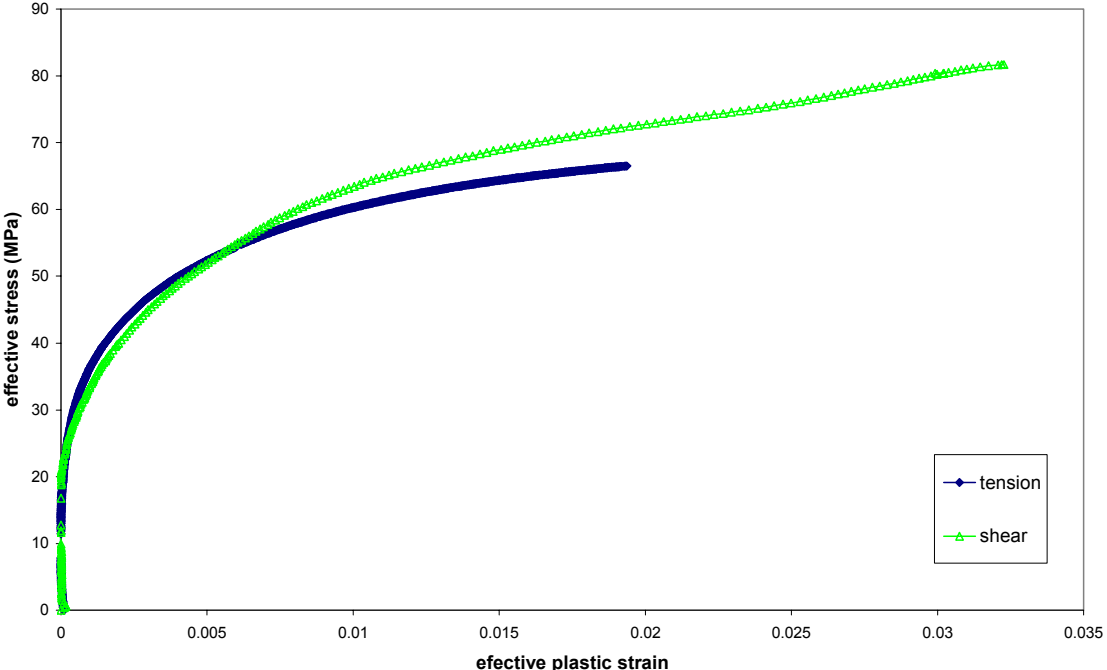


Figure 14. Measured stress/strain data for tension and shear plotted on axes of effective stress against effective plastic strain. Data were measured at the same effective plastic strain rate of 1.10⁻⁴ s⁻¹ at 0°C.

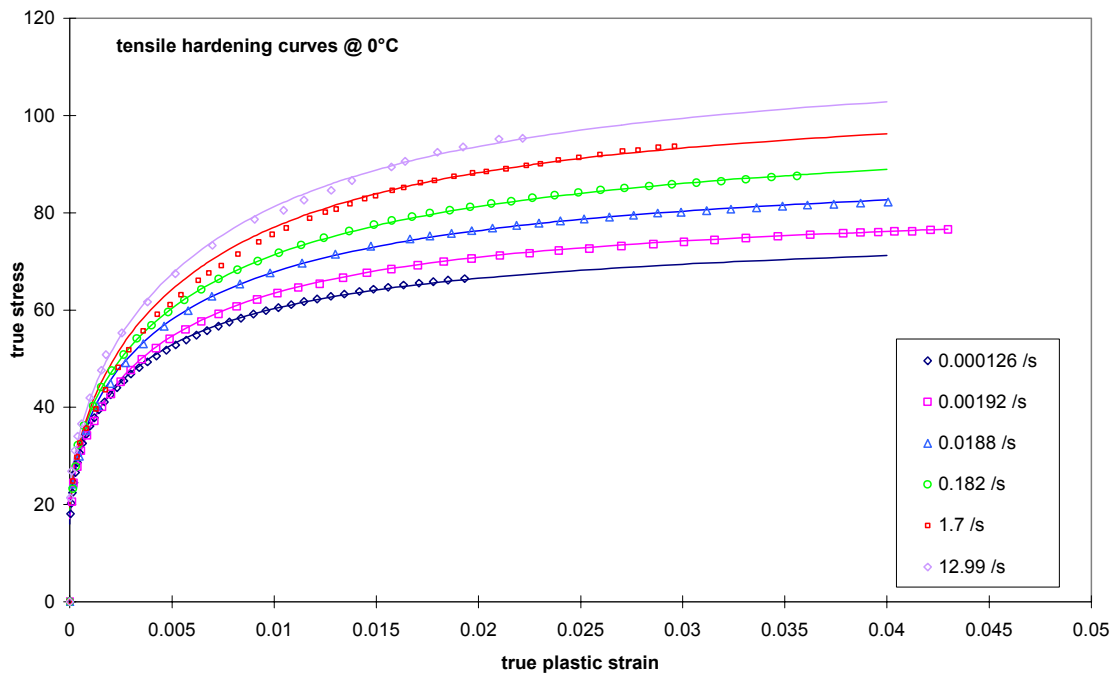


Figure 15. Measured rate-dependent hardening curves for the epoxy adhesive at 0°C. The continuous curves are fits to the data.

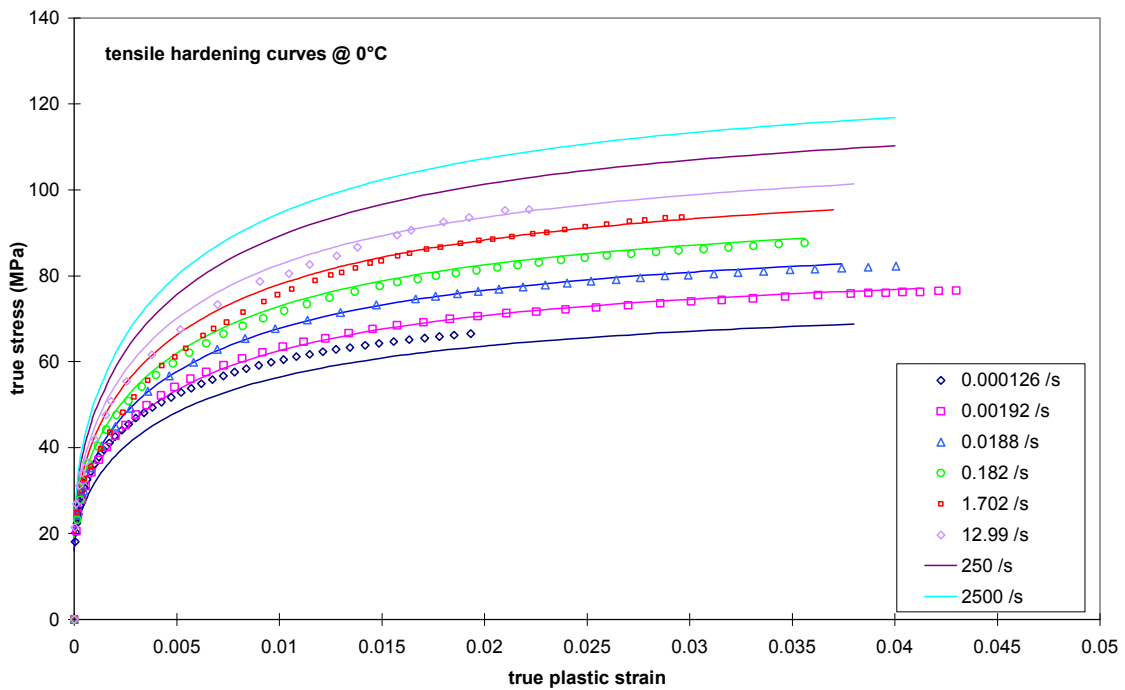


Figure 16. Comparison of 0°C measured data (symbols) and fitted hardening curves (solid lines) derived using equation 16 and averaged parameters. Also shown are extrapolated data for strain rates of 250 s⁻¹ and 2500 s⁻¹.

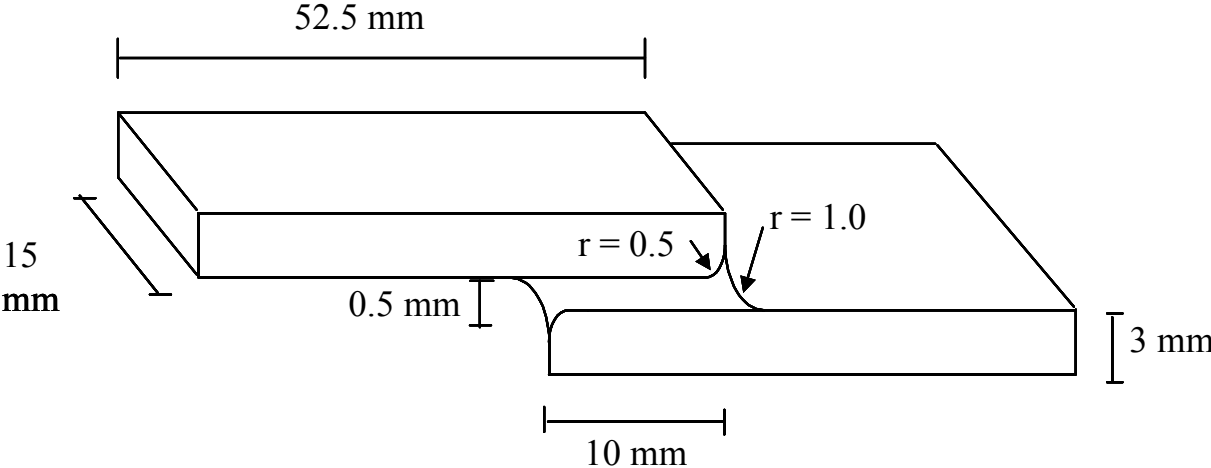


Figure 17. A schematic diagram of the lap-joint test specimen.

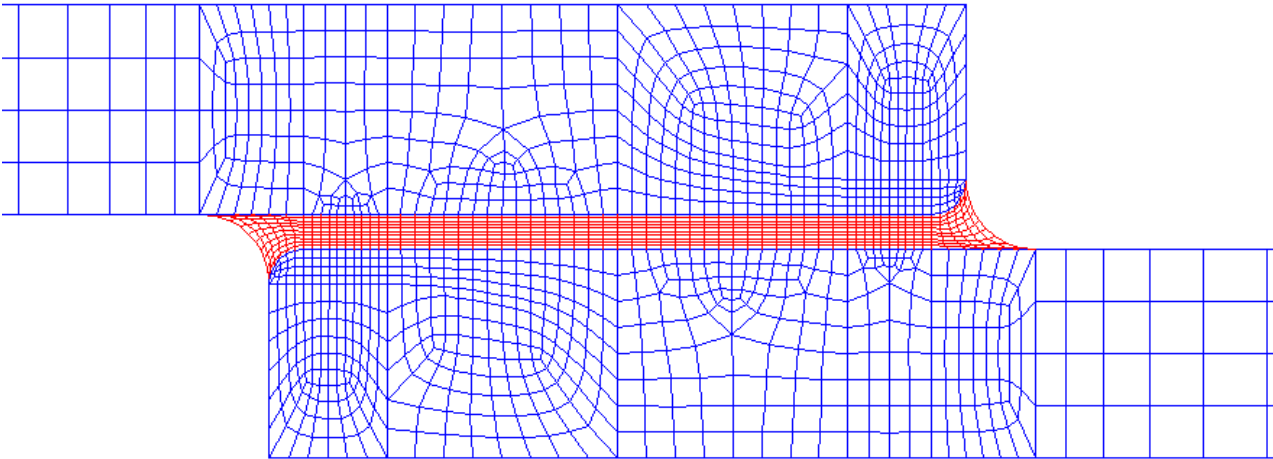


Figure 18. Mesh used for FE analysis of the lap-joint specimen.

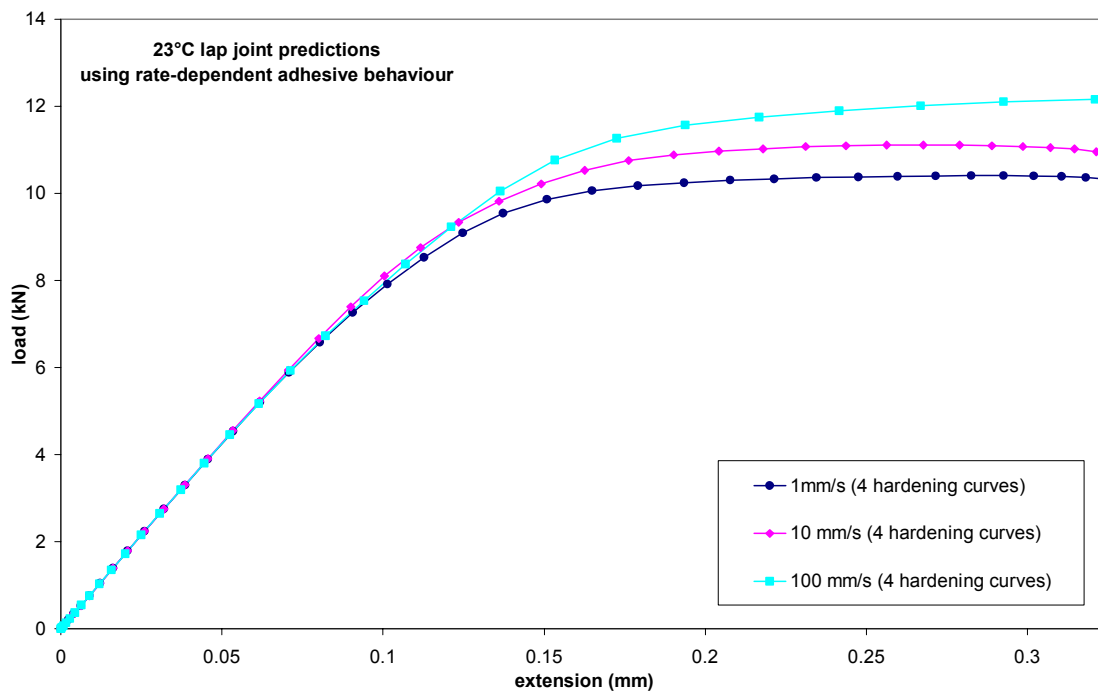


Figure 19. Predictions of lap-joint behaviour at 23°C using the linear Drucker-Prager model with rate-dependent plasticity and the explicit solver.

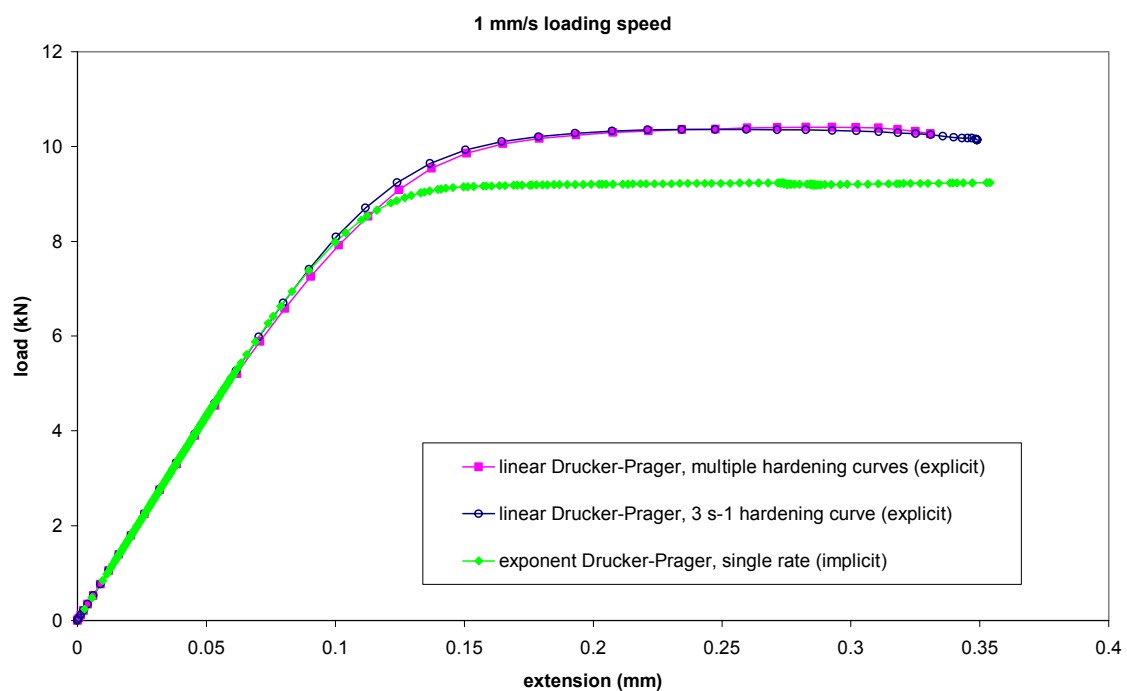


Figure 20. Comparison of the 1 mm/s force/extension prediction from a linear Drucker-Prager analysis with rate-dependent plasticity with the equivalent prediction obtained using a single strain rate hardening curve (3 s^{-1}). Also shown is the exponent Drucker-Prager prediction made with the same single strain rate hardening curve.

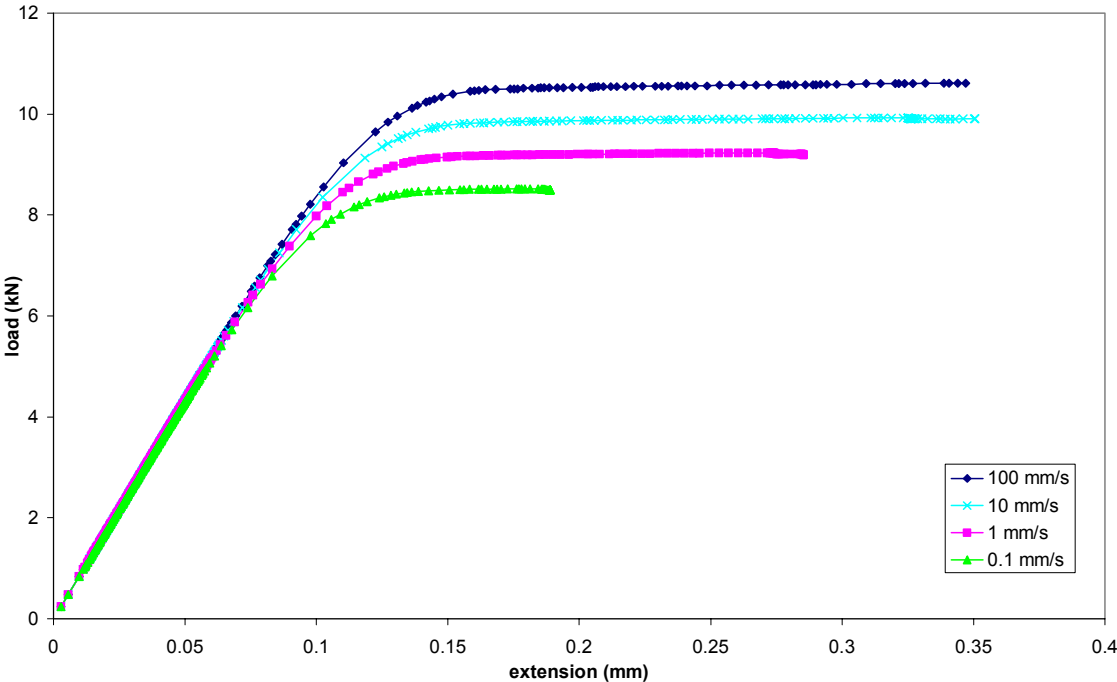


Figure 21. Exponent Drucker-Prager predictions of 23°C lap-joint behaviour obtained using the relevant single rate hardening curve.

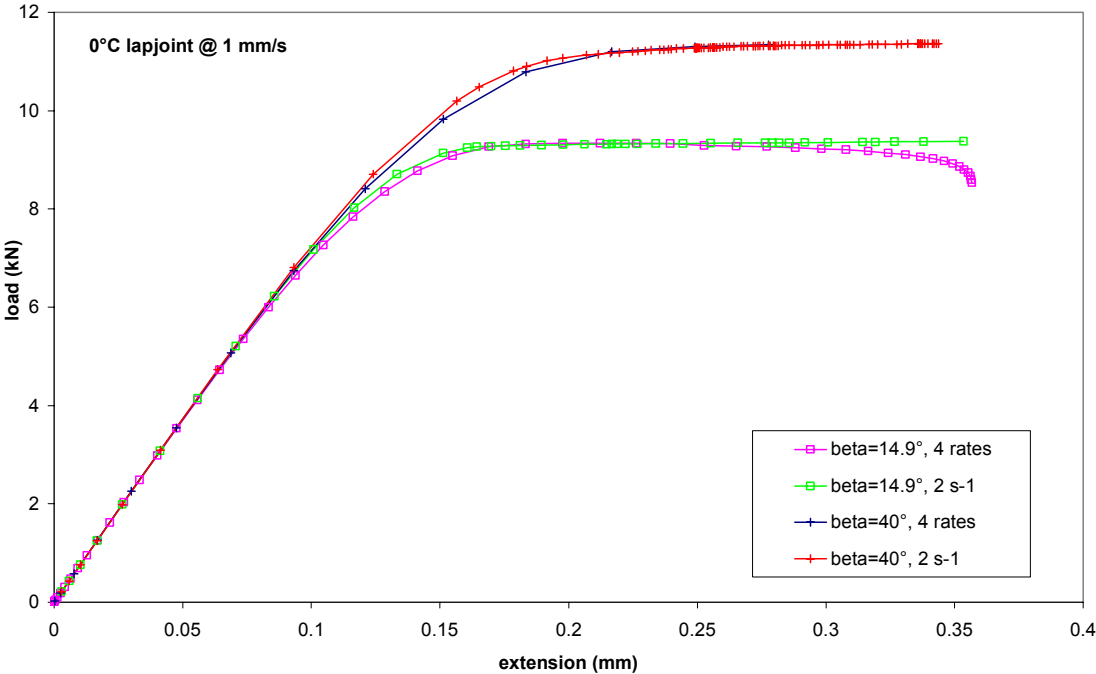
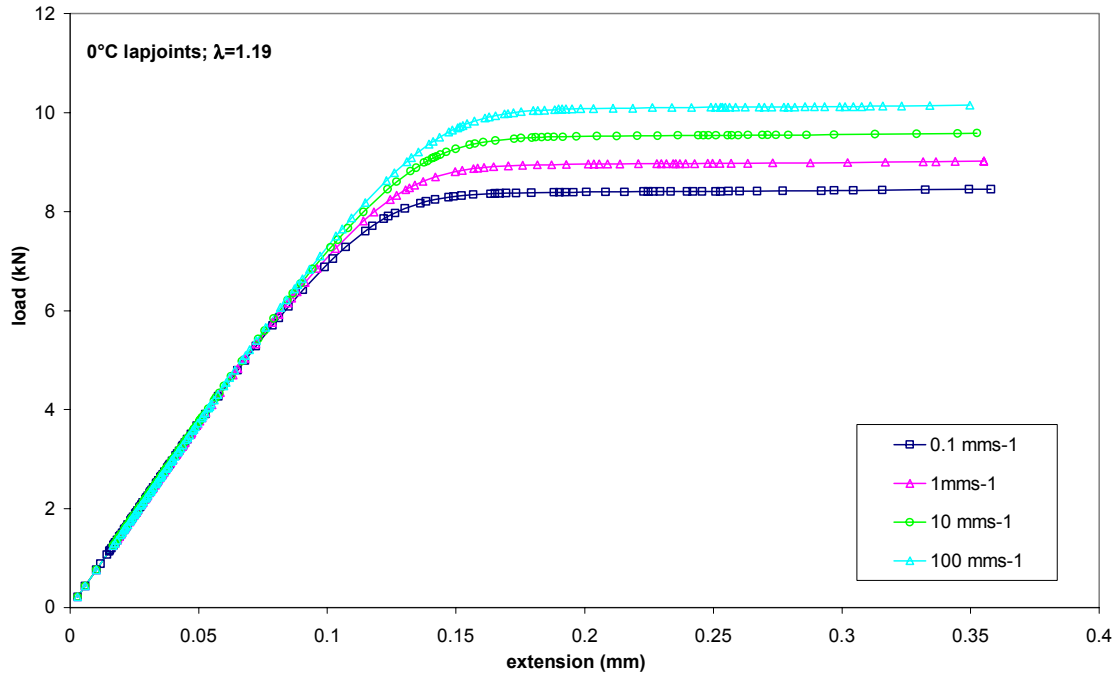
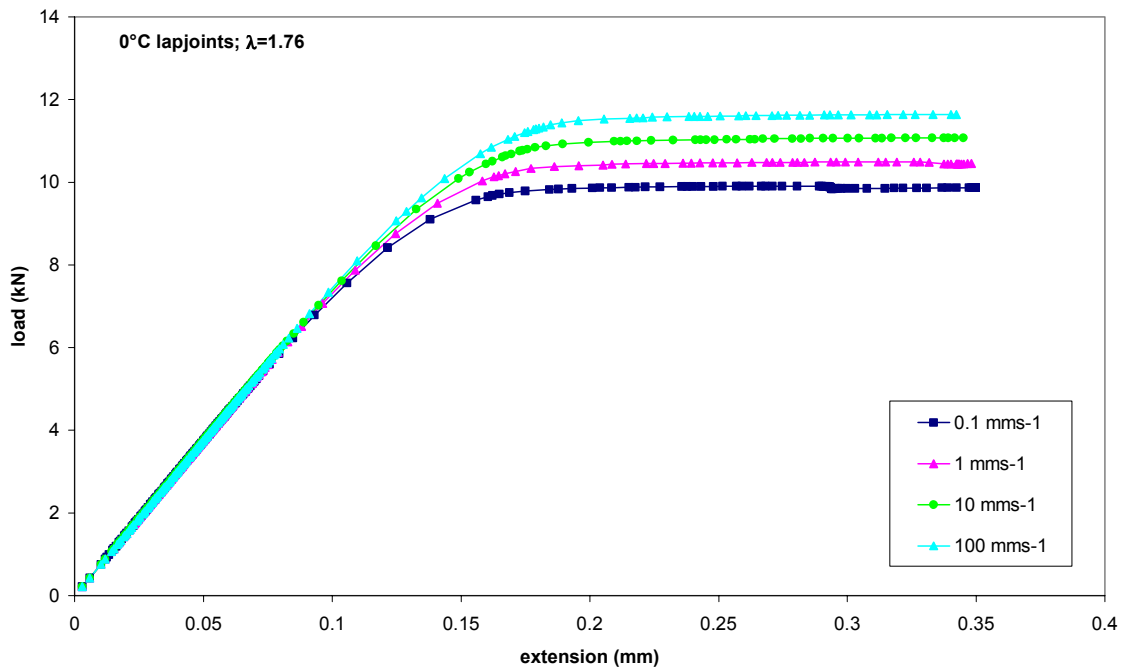


Figure 22. Predictions of 0°C lap-joint behaviour at a speed of 1 mm/s using two different sets of linear Drucker-Prager parameters and the explicit solver. Analyses with the relevant single rate hardening curves are compared to those obtained with multiple hardening curves.

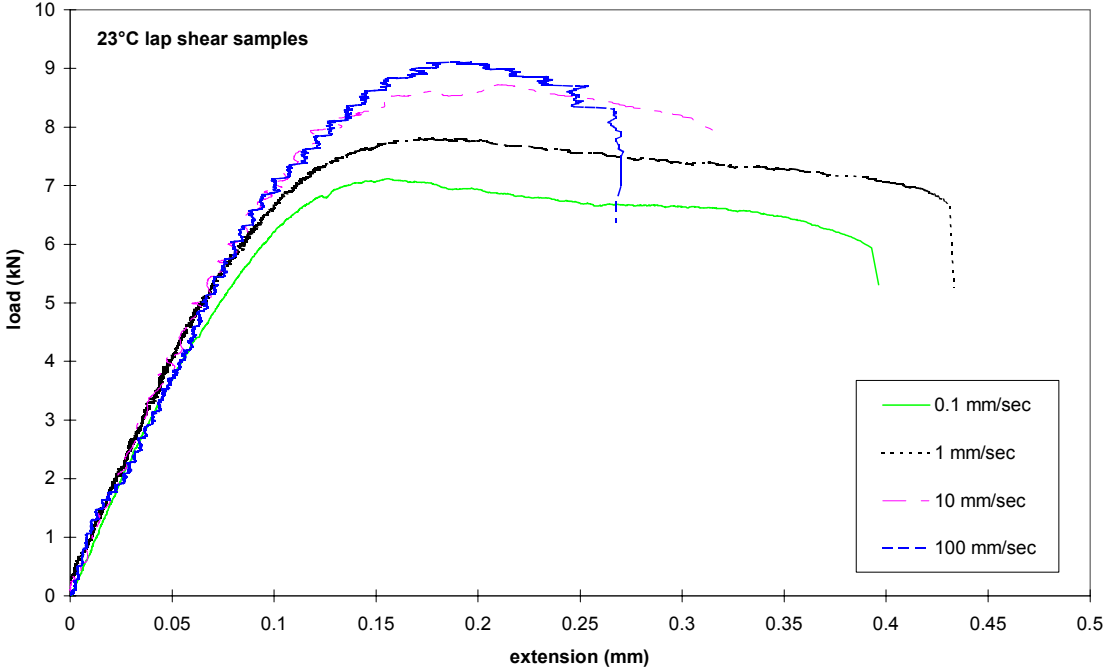


(a)

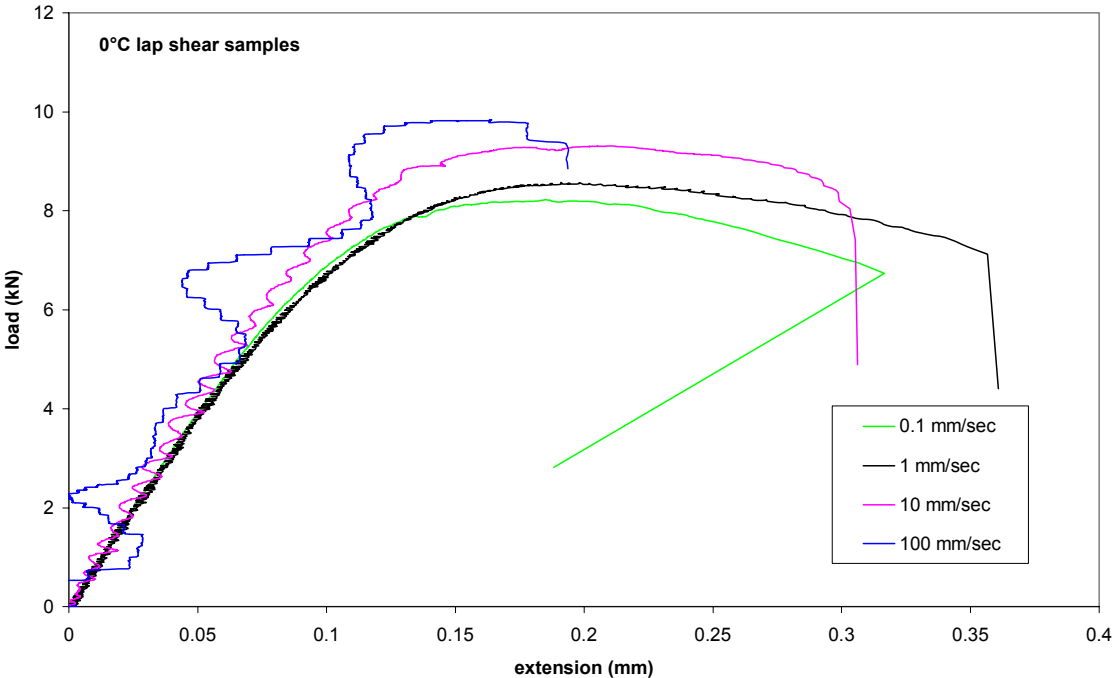


(b)

Figure 23. Predictions of lap-joint behaviour at 0°C using the exponent Drucker-Prager model with (a) coefficients obtained with $\lambda = 1.19$ and (b) coefficients obtained with $\lambda = 1.76$. Both analyses sets are run with the equivalent single strain rate hardening curves.



(a)



(b)

Figure 24. Experimental force/extension curves obtained for lap-joint specimen tested at (a) 23°C and (b) 0°C at speeds of between 0.1 mm/s and 100 mm/s.

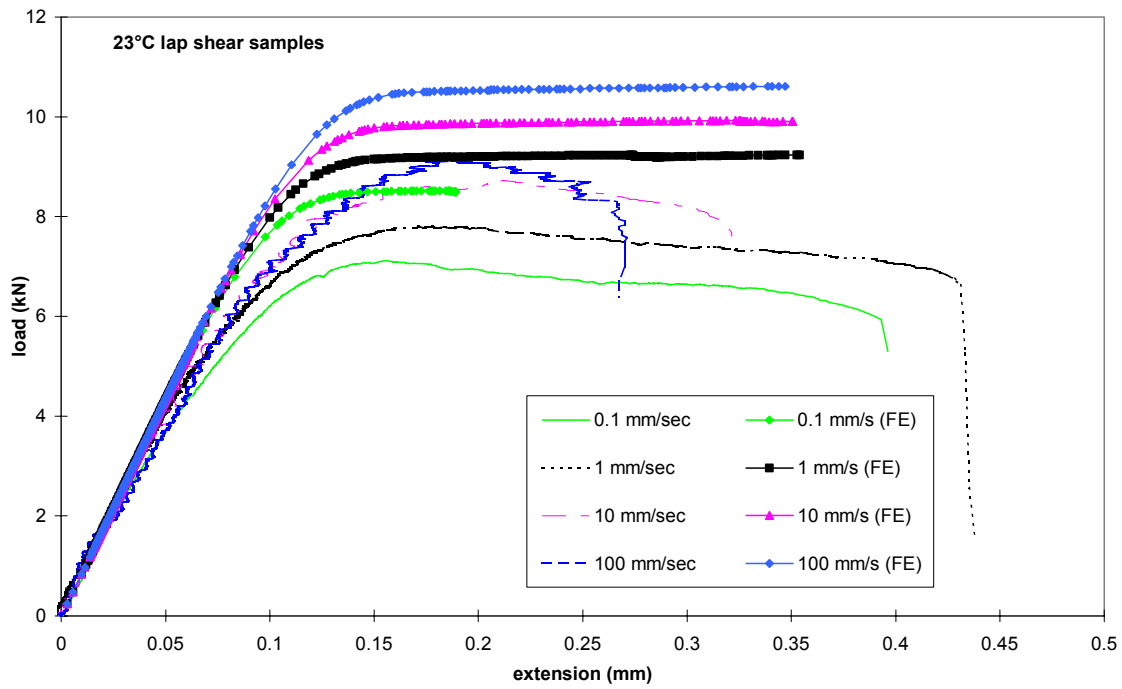


Figure 25. Comparison of predicted and measured force/extension curves for lap-joint specimens tested at 23°C over a range of loading speeds.

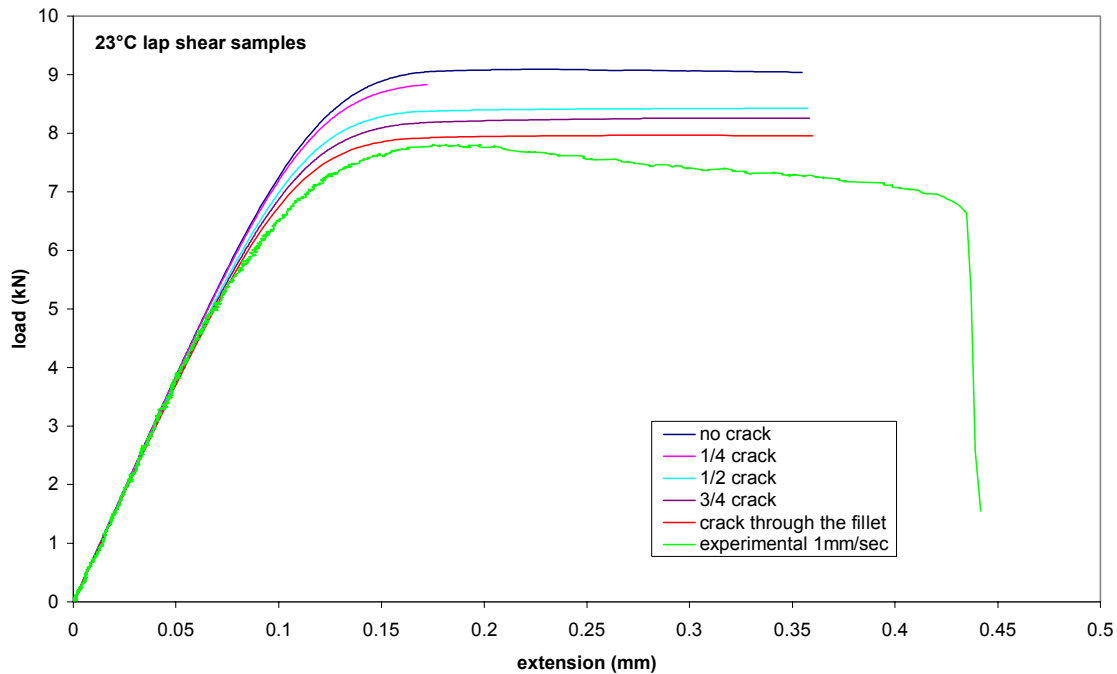


Figure 26. Comparison of the 23°C experimental force/extension curve at 0.1 mm/s with predictions obtained with meshes containing various length cracks between the adhesive and adherend. Exponent Drucker-Prager model with single hardening curve (0.3 s^{-1}).

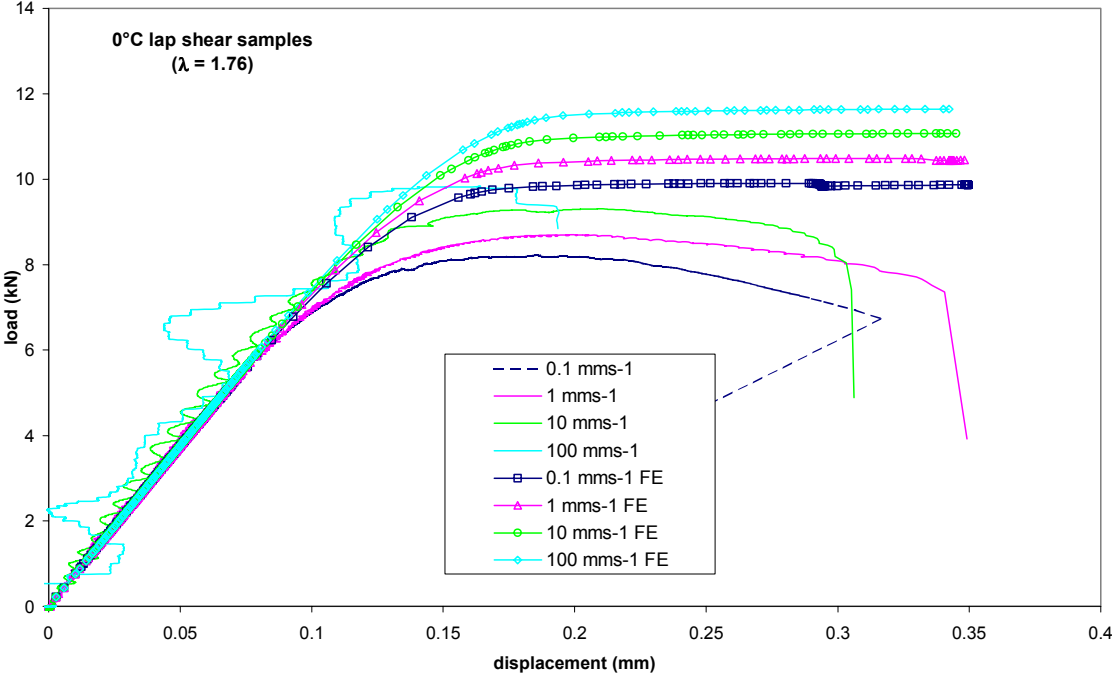


Figure 27. Comparison of force/extension curves measured at 0°C with predictions obtained using exponent Drucker-Prager parameters calculated from derived 0°C shear data.

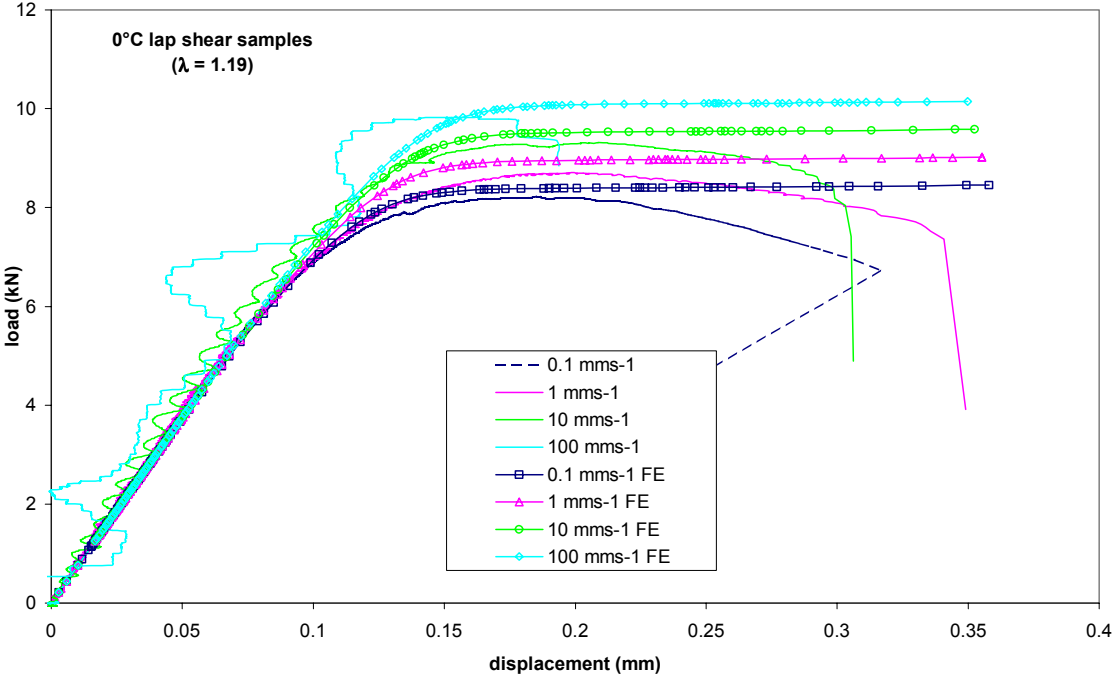


Figure 28. Comparison of force/extension curves measured at 0°C with predictions obtained using exponent Drucker-Prager parameters calculated from measured 0°C shear data.